



**HAL**  
open science

# Diagrammatic theory of magnetic and quadrupolar contributions to sum-frequency generation in composite systems

Thomas Noblet, Bertrand Busson

► **To cite this version:**

Thomas Noblet, Bertrand Busson. Diagrammatic theory of magnetic and quadrupolar contributions to sum-frequency generation in composite systems. *Journal of Chemical Physics*, 2024, 160 (2), pp.024704. 10.1063/5.0187520 . hal-04382361

**HAL Id: hal-04382361**

**<https://hal.science/hal-04382361>**

Submitted on 9 Jan 2024

**HAL** is a multi-disciplinary open access archive for the deposit and dissemination of scientific research documents, whether they are published or not. The documents may come from teaching and research institutions in France or abroad, or from public or private research centers.

L'archive ouverte pluridisciplinaire **HAL**, est destinée au dépôt et à la diffusion de documents scientifiques de niveau recherche, publiés ou non, émanant des établissements d'enseignement et de recherche français ou étrangers, des laboratoires publics ou privés.

# Diagrammatic Theory of Magnetic and Quadrupolar Contributions to Sum-Frequency Generation in Composite Systems

Thomas Noblet<sup>1</sup> and Bertrand Busson<sup>2</sup>

<sup>1</sup>*GRASP-Biophotonics, CESAM, University of Liege, Institute of Physics, Allée du 6 août 17, 4000 Liège, Belgium.*<sup>a)</sup>

<sup>2</sup>*Université Paris-Saclay, CNRS, Institut de Chimie Physique, UMR 8000, 91405 ORSAY, France*

(Dated: 12 December 2023)

Second-order nonlinear processes like Sum-Frequency Generation (SFG) are essentially defined in the electric dipolar approximation. However, when dealing with the SFG responses of a bulk, big nanoparticles, highly symmetric objects or chiral species, magnetic and quadrupolar contributions play a significant role in the process too. We extend the diagrammatic theory for linear and nonlinear optics to include these terms for single objects as well as for multipartite systems in interaction. Magnetic and quadrupolar quantities are introduced in the formalism as incoming fields, interaction intermediates and sources of optical nonlinearity. New response functions and complex nonlinear processes are defined, and their symmetry properties are analyzed. This leads to a focus on several kinds of applications involving nanoscale coupled objects, symmetric molecular systems and chiral materials, both in line with the existing literature and opening new possibilities for original complex systems.

---

<sup>a)</sup>Electronic mail: t.noblet@uliege.be

## I. INTRODUCTION

Second-order nonlinear optical processes like Second Harmonic Generation (SHG) and Sum-Frequency Generation (SFG) are usually exploited for their symmetry properties making them intrinsically specific to interfaces.<sup>1</sup> In particular, SFG can be experimentally designed to perform surface-specific infrared-visible spectroscopy and thus finely probe vibrational and vibronic properties of molecular species. Even if it is possible to extract a spectroscopic response characteristic of the interface only, the surface-related signal is sometimes perturbed by the presence of additional sources of SFG, arising from the underlying bulk<sup>2</sup> (e.g. substrate) or a subjacent multilayered structure.<sup>3,4</sup> Interference between surface and substrate signals may be experimentally suppressed<sup>5</sup> or conversely exploited to access phase information.<sup>6,7</sup> Other distortions of the SFG signals stem from the interaction between the probed molecules and their local environment, which can be made of various coupled entities, from fellow molecules (in homogeneous samples) to organic and inorganic partners (in composite materials). Such couplings are usually controlled by the experimenter and may even allow the characterization of additional information (e.g. molecular packing in a dense monolayer<sup>8</sup>) or the enhancement of the molecular SFG response through coupling to nanoscale objects like nanoparticles<sup>9</sup> or semiconductor quantum dots.<sup>10</sup>

A general diagrammatic theory has been established,<sup>11</sup> based on Matsubara loop diagrams and governed by Feynman rules, for the description and calculation of the SFG processes involving interactions between molecules and their partners. Even if our loop diagrams and the usual doubled-sided diagrams both succeed in describing the response functions of one isolated entity, double-sided diagrams fail to account for composite systems because the combination of two or more double-sided diagrams is not a double-sided diagram. On the contrary, our formalism allows to combine an arbitrary number of interconnected loop diagrams into one loop diagram representing the system as a whole. This approach has been successfully applied to the molecule-nanoparticle systems to account for plasmon-enhanced vibrational SFG spectroscopy.<sup>12</sup> In this case, electric dipole-dipole coupling between molecules and particles was postulated, as usual in the description of the optical response of complex systems.<sup>8,13,14</sup> This corresponds to the first-order contribution to the multipolar perturbative expansion of the electromagnetic interaction.<sup>15</sup> The higher orders, among which the magnetic and quadrupolar terms are the leading contributions,

are usually neglected on the basis of their weaknesses. However, the purely electric dipolar approximation cannot be considered as a general prescription, as shows the example of the Mie theory for spheres<sup>16</sup> which requires to sum up all the multipolar orders. Besides, modeling the SHG and SFG responses needs to include quadrupolar and magnetic terms in various cases: metallic substrates,<sup>17</sup> liquid bulks,<sup>18,19</sup> nanoparticles.<sup>20–23</sup> For example, the SFG signal originating from the water bending mode has been ascribed to a quadrupolar process,<sup>24–26</sup> even if there is still an ongoing debate on this point.<sup>27</sup> This is especially important for bulk contributions to second-order nonlinear optics,<sup>28,29</sup> where the electric dipole terms vanish while the magnetic and quadrupolar ones do not. The weaknesses of these responses may be compensated by the bigger amount of matter probed, in particular in transmission geometry where the phase mismatch is more favorable than in reflection,<sup>30,31</sup> as well as by high electric field gradients, related to the discontinuity of material properties at the interface between two bulks<sup>32,33</sup> or to the fast amplitude decay of the electric field inside a nontransparent material.<sup>34</sup> As for chiral objects, their optical activity is known to originate in the interaction between electric and magnetic dipolar excitations,<sup>35,36</sup> either intra- or intermolecular.<sup>37,38</sup>

In this paper, we extend the Feynman-Matsubara diagrammatic description of linear and nonlinear optical response functions to include magnetic and quadrupolar contributions at all stages. This implies to consider (i) magnetic fields and electric field gradients as vectors of light-matter interactions, (ii) magnetic and quadrupolar molecule-partner interaction Hamiltonians, and (iii) magnetic dipoles and electric quadrupoles as sources of SFG radiation. As a consequence, new first- and second-order response functions are defined, which calculations require to involve magnetic dipole and electric quadrupole transition probabilities. Even if these are usually considered weak (about one percent of the electric dipole ones<sup>39</sup>), they can become the main allowed transitions for symmetry reasons.<sup>19,40</sup> The molecule-partner diagrams are factored by these new response functions, connected through energy transfer coefficients. We thus enumerate and sort all the relevant diagrams, then discuss their practical consequences for SFG spectroscopy in the cases of various bipartite molecule-partner systems, according to their local and global geometries and to the nature of the partner coupled to the molecules.

## II. ELEMENTARY RESPONSE FUNCTIONS

Before considering the bipartite diagrams describing the response functions of molecule-partner composite systems, we must pay a special attention to the definition of the elementary response functions describing a single object, whether it is the molecule or any quantum object playing the role of its partner in the following sections. Considered as a set of  $N$  electrons whose position operators are  $\{\hat{\mathbf{r}}_\nu\}_{\nu=1}^N$ , a microscopic entity is characterized by three operators: the electric dipole moment  $\hat{\mathbf{p}}$ , the electric quadrupole moment  $\hat{\mathbf{q}}$ , and the magnetic moment  $\hat{\boldsymbol{\mu}}$ . They constitute the main basis on which the optical behavior of a microscopic system is described and are respectively defined as:

$$\hat{\mathbf{p}} = \sum_{\nu=1}^N e\hat{\mathbf{r}}_\nu, \quad \hat{\mathbf{q}} = \sum_{\nu=1}^N e\hat{\mathbf{r}}_\nu^t \hat{\mathbf{r}}_\nu, \quad \text{and} \quad \hat{\boldsymbol{\mu}} = \gamma(\hat{\mathbf{L}} + g_s\hat{\mathbf{S}}), \quad (1)$$

where  $\hat{\mathbf{L}} = \sum_{\nu=1}^N \hat{\mathbf{r}}_\nu \times \hat{\mathbf{p}}_\nu$  and  $\hat{\mathbf{S}}$  are the total orbital and spin angular momenta of the electrons,  $\hat{\mathbf{p}}_\nu$  the momentum operator,  $\gamma = e/2m$  the gyromagnetic ratio, and  $g_s = 2$  the electron Landé  $g$ -factor.<sup>35,41,42</sup>

At first and second orders in the source fields, these electric and magnetic moments are driven by linear polarizabilities  $\boldsymbol{\alpha}$  and first nonlinear hyperpolarizabilities  $\boldsymbol{\beta}$ . At the electric dipolar level, the polarizability  $\boldsymbol{\alpha}^{\text{ee}}$  relates the excitation electric field  $\mathbf{E}$  to the response dipole moment  $\mathbf{p} = \langle \hat{\mathbf{p}} \rangle$  through  $p_i(\omega) = \sum_j \alpha_{ij}^{\text{ee}}(\omega) E_j(\omega)$ . In the SFG process, the hyperpolarizability  $\boldsymbol{\beta}^{\text{eee}}$  mixes two sources  $\mathbf{E}(\omega_1)$  and  $\mathbf{E}(\omega_2)$  to generate an electric dipole at frequency  $\omega_3 = \omega_1 + \omega_2$ , given by  $p_i(\omega_3) = \sum_{j,k} \beta_{ijk}^{\text{eee}}(\omega_1, \omega_2) E_j(\omega_1) E_k(\omega_2)$ .

In terms of loop diagrams, both quantities have been drawn (Fig. 1a and b) and calculated in previous papers according to the Feynman rules dedicated to optical response functions.<sup>11,12</sup> They encompass two and three vertices, respectively, representing light-matter interactions at the electric dipole level, thus governed by the Hamiltonian  $\mathcal{H}^e = -\hat{\mathbf{p}} \cdot \mathbf{E}$ . For the polarizability  $\boldsymbol{\alpha}^{\text{ee}}(\omega)$ , we have:

$$\alpha_{ij}^{\text{ee}}(\omega) = \frac{1}{\hbar} \sum_{m,n} \hat{\rho}_{mm} \left( \frac{p_{nm}^i p_{mn}^j}{\omega + \omega_{nm} + i\Gamma_{nm}} - \frac{p_{nm}^j p_{mn}^i}{\omega - \omega_{nm} + i\Gamma_{nm}} \right). \quad (2)$$

where  $\{i, j\}$  stand for the Cartesian coordinates  $\{x, y, z\}$ ,  $p_{nm}^i = \langle n | \hat{p}_i | m \rangle$  represents the transition electric dipole moment along the  $i$ -direction between states  $|m\rangle$  and  $|n\rangle$  (charac-

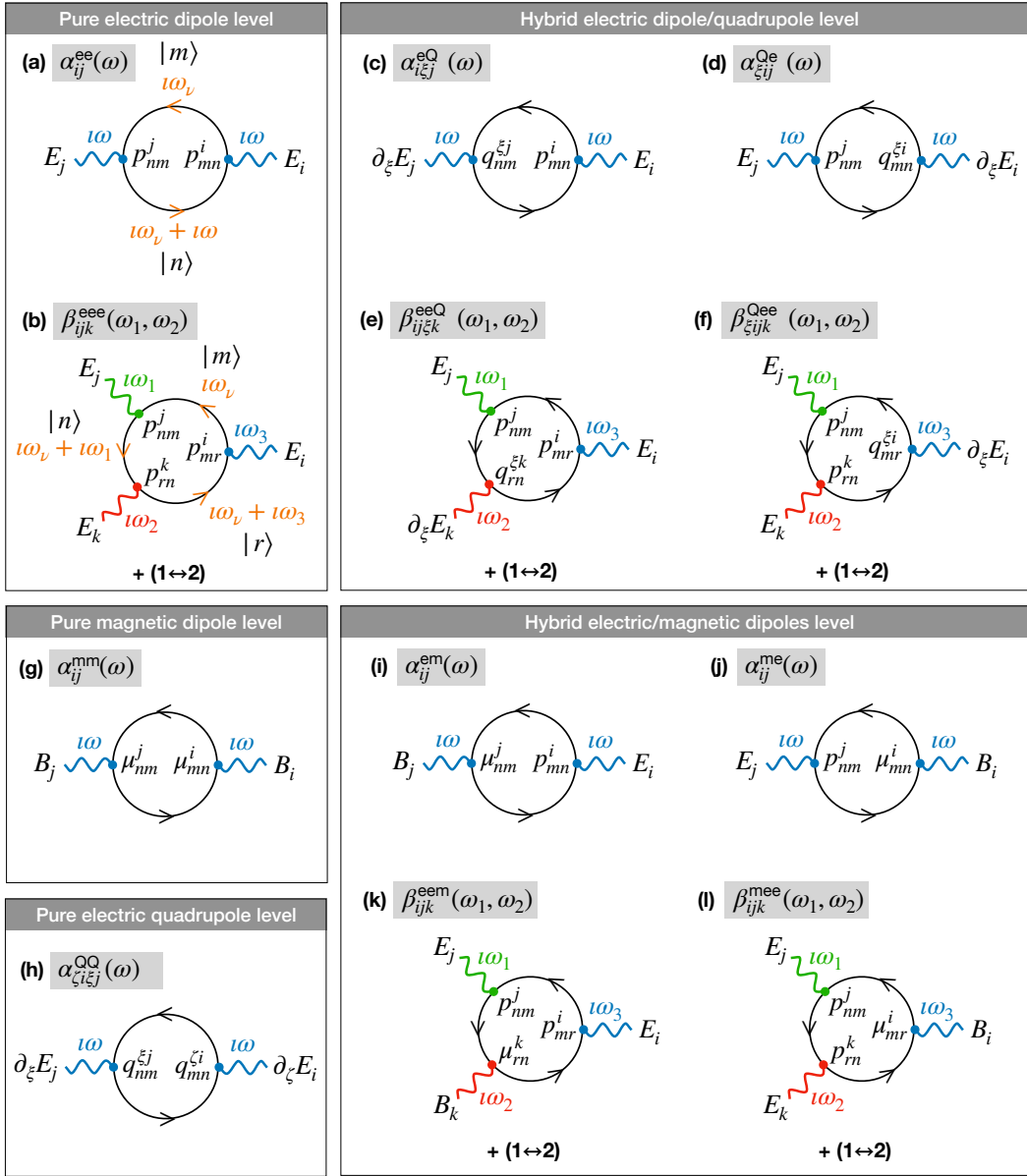


FIG. 1. Loop diagrams of elementary response functions. (a) Linear polarizability  $\alpha^{ee}$  and (b) first hyperpolarizability  $\beta^{eee}$  of a simple system at the pure electric dipole level. These two diagrams define the frequency filling of the propagators associated with the states  $|m\rangle$ ,  $|n\rangle$  and  $|r\rangle$  which also applies to the others. Linear polarizabilities (c)  $\alpha^{eQ}$  and (d)  $\alpha^{Qe}$  involving an input and an output quadrupolar vertex, respectively. Hyperpolarizabilities (e)  $\beta^{eeQ}$  and (f)  $\beta^{Qee}$  involving an  $\omega_2$ -input and an  $\omega_3$ -output quadrupolar vertex, respectively. The hyperpolarizability  $\beta^{eQe}$  is obtained from ‘eeQ’ by applying the gradient  $\partial_{\xi}$  on  $E_j$  (instead of  $E_k$ ) and placing the quadrupolar interaction on the corresponding vertex. (g) Linear polarizability  $\alpha^{mm}$  at the pure magnetic level. (h) Linear polarizability  $\alpha^{QQ}$  at the pure quadrupolar level. Linear polarizabilities (i)  $\alpha^{em}$  and (j)  $\alpha^{me}$  involving an input and an output magnetic vertex, respectively. Hyperpolarizabilities (k)  $\beta^{eem}$  and (l)  $\beta^{mee}$  involving an  $\omega_2$ -input and an  $\omega_3$ -output magnetic vertex, respectively. The hyperpolarizability  $\beta^{eme}$  is obtained from ‘eem’ by considering the input field  $B_j$  instead of  $E_j$  and placing the magnetic interaction on the corresponding vertex. For all hyperpolarizabilities, we must consider a second diagram obtained through the permutation of the two input photons ( $1 \leftrightarrow 2$ ) to recover the complete response function  $\beta_{ijk}$ .

terized by the energy difference  $\hbar\omega_{nm} = \hbar\omega_n - \hbar\omega_m$  and the transition linewidth  $\Gamma_{nm}$ ), and  $\hat{\rho}_{mm}$  is the density matrix diagonal element related to state  $|m\rangle$ . The equivalence between  $\hat{\rho}_{mm}$  and the Fermi-Dirac distribution  $\rho(\omega_m)$  at energy  $\hbar\omega_m$  has been used.<sup>11</sup> The response function  $\beta_{ijk}^{\text{eee}}(\omega_1, \omega_2)$  is expressed as a function of imaginary frequencies (which are natural as far as Feynman-Matsubara formalism is concerned) and encompasses six terms:

$$\beta_{ijk}^{\text{eee}}(\omega_1, \omega_2) = \frac{1}{\hbar^2} \sum_{m,n,r} \hat{\rho}_{rr} \left[ \frac{p_{rn}^i p_{nm}^j p_{mr}^k}{(\omega_{nr} - i\omega_3)(\omega_{mr} - i\omega_2)} + \frac{p_{mn}^i p_{nr}^j p_{rm}^k}{(\omega_{rm} - i\omega_2)(\omega_{rn} + i\omega_1)} \right. \\ \left. + \frac{p_{mr}^i p_{rn}^j p_{nm}^k}{(\omega_{mr} + i\omega_3)(\omega_{nr} + i\omega_1)} + \frac{p_{rn}^i p_{nr}^j p_{nm}^k}{(\omega_{nr} - i\omega_3)(\omega_{mr} - i\omega_1)} \right. \\ \left. + \frac{p_{mn}^i p_{rm}^j p_{nr}^k}{(\omega_{rm} - i\omega_1)(\omega_{rn} + i\omega_2)} + \frac{p_{mr}^i p_{nm}^j p_{rn}^k}{(\omega_{mr} + i\omega_3)(\omega_{nr} + i\omega_2)} \right]. \quad (3)$$

They give birth to the usual eight terms of the literature, and the response function in real frequencies follows from analytic continuity.<sup>11</sup> Appendix A provides a summary of the method enabling to translate the drawing of a loop diagram into the analytical expression of the associated response function.

Here we consider alternate response functions for which one of the vertices involves a magnetic or a quadrupolar interaction, respectively described by the Hamiltonians  $\mathcal{H}^m = -\hat{\boldsymbol{\mu}} \cdot \mathbf{B}$  and  $\mathcal{H}^Q = -\frac{1}{2} \sum_{i,j} \hat{q}_{ij} \partial_j E_i = -\frac{1}{2} (\hat{\mathbf{q}} \nabla) \cdot \mathbf{E}$ , with  $\nabla = {}^t(\partial_x, \partial_y, \partial_z)$ , encoding how the magnetic moment  $\boldsymbol{\mu} = \langle \hat{\boldsymbol{\mu}} \rangle$  interacts with a magnetic field  $\mathbf{B}$  and the quadrupole moment  $\mathbf{q} = \langle \hat{\mathbf{q}} \rangle$  with electric field gradients  $\partial_j E_i$ , respectively.<sup>43</sup> These additional responses are usually small as compared to the electric dipole terms, but may become measurable in some cases as detailed in the Introduction. Throughout the paper, the superscripts ‘e’, ‘m’ and ‘Q’ stand for ‘electric dipole’, ‘magnetic dipole’ and ‘electric quadrupole’, respectively. Note that the quadrupole superscript is in capital in order to remind that it involves a rank-2 tensor while the electric and magnetic dipoles involve rank-1 tensors. The tensor dimension of the response functions will indeed depend on the natures of the associated moments.

As for the linear response, it is possible to draw simple (em) and (eQ) diagrams and convert them into response functions. In Fig. 1i and j, we define the rank-2 response functions  $\boldsymbol{\alpha}^{\text{em}}$  and  $\boldsymbol{\alpha}^{\text{me}}$  by  $p_i = \sum_j \alpha_{ij}^{\text{em}} B_j$  and  $\mu_i = \sum_j \alpha_{ij}^{\text{me}} E_j$ . These hybrid functions transform a magnetic (resp. electric) excitation by light into an electric (resp. magnetic) response.<sup>44–48</sup> In the same way, the first order rank-3 response functions  $\boldsymbol{\alpha}^{\text{eQ}}$  and  $\boldsymbol{\alpha}^{\text{Qe}}$  (Fig. 1c and d) mix the electric and quadrupole sources ( $E_j$  or  $\partial_\xi E_j$ ) and responses ( $p_i$  or  $q_{\xi i}$ ) through

$p_i = \sum_{\xi,j} \alpha_{i\xi j}^{eQ} \partial_\xi E_j$  and  $q_{\xi i} = \sum_j \alpha_{\xi i j}^{Qe} E_j$ , where  $\xi$  depicts the Cartesian coordinate along which the field gradient is assessed.<sup>49,50</sup> The values of all these response functions flow from the calculation of their loop diagrams following the twelve Feynman rules. We provide a detailed example for  $\alpha^{em}$  and  $\alpha^{eQ}$  in Appendix B, together with the results for the others. It essentially turns out that the response functions  $\alpha^{em}$ ,  $\alpha^{me}$ ,  $\alpha^{eQ}$  and  $\alpha^{Qe}$  can be deduced from Eq. (2) by simple manipulations of the transition dipole moments. As discussed later, (em/me) and (eQ/Qe) response functions are forbidden for centrosymmetric objects and bulks.

In order to address the centrosymmetric case, it is also possible to define a purely magnetic linear polarizability  $\alpha^{mm}$  (Fig. 1g) accounting for the generation of a magnetic moment  $\boldsymbol{\mu}$  after a  $\mathbf{B}$  excitation:  $\mu_i(\omega) = \sum_j \alpha_{ij}^{mm}(\omega) B_j(\omega)$ . This (mm) polarizability is an optical response function characterizing the generation of an induced microscopic moment  $\boldsymbol{\mu}$  in response to the magnetic component of an electromagnetic wave, hence oscillating at an optical frequency. It must be distinguished from the magnetic susceptibility defined for magnetic materials with respect to their macroscopic magnetization. In the same way, the quadrupolar response function  $\alpha^{QQ}$  is defined as  $q_{\xi i} = \sum_{\zeta,j} \alpha_{\xi i \zeta j}^{QQ} \partial_\zeta E_j$  (Fig. 1h). Both  $\alpha^{mm}$  and  $\alpha^{QQ}$  are introduced here in order to ensure compliance with the lowest orders of Mie theory. As we shall see below, their use is mostly restricted to systems involving a spherical partner. In that particular case,  $\alpha^{QQ}$  may be accounted for by an equivalent isotropic scalar quadrupolarizability.<sup>49</sup> For lower symmetries, they are superseded by  $\alpha^{em}$ ,  $\alpha^{me}$ ,  $\alpha^{eQ}$  and  $\alpha^{Qe}$ .

Following the example of first-order functions, we define a new set of second-order response functions in order to account for magnetic and quadrupolar light-matter interactions. We limit ourselves to elementary SFG processes for which one interaction at most differs

from the electric dipole Hamiltonian. Hence we have:

$$\begin{aligned}
p_i(\omega_3) = & \sum_{jk} \left[ \beta_{ijk}^{eee}(\omega_1, \omega_2) E_j(\omega_1) E_k(\omega_2) \right. \\
& + \beta_{ijk}^{eem}(\omega_1, \omega_2) E_j(\omega_1) B_k(\omega_2) + \beta_{ijk}^{eme}(\omega_1, \omega_2) B_j(\omega_1) E_k(\omega_2) \\
& \left. + \sum_{\xi} \beta_{ij\xi k}^{eeQ}(\omega_1, \omega_2) E_j(\omega_1) \partial_{\xi} E_k(\omega_2) + \beta_{i\xi jk}^{eQe}(\omega_1, \omega_2) \partial_{\xi} E_j(\omega_1) E_k(\omega_2) \right], \quad (4)
\end{aligned}$$

$$\mu_i(\omega_3) = \sum_{jk} \beta_{ijk}^{mee}(\omega_1, \omega_2) E_j(\omega_1) E_k(\omega_2), \quad (5)$$

$$q_{\xi i}(\omega_3) = \sum_{jk} \beta_{\xi jk}^{Qee}(\omega_1, \omega_2) E_j(\omega_1) E_k(\omega_2). \quad (6)$$

These alternate second-order elementary functions<sup>2,33,51,52</sup> are more described in the literature than their first-order counterparts. From symmetry reasons, the fully electric-dipole functions  $\beta^{eee}$  vanish in a centrosymmetric bulk, while the others do not. Even if the leading (eee) SFG process is most of the times recorded precisely for its surface specificity (in order to extract an optical signature of the interfaces where this centrosymmetry is broken), the other contributions from the bulk often mix with the surface ones<sup>6,30,53</sup> and have their own interest.<sup>17,19</sup> In other words, the hierarchy between the (eee), (eem/eme/mee) and (eeQ/eQe/Qee)  $\beta$  functions (in terms of perturbative expansion with respect to the field amplitude) is softer because of the different selection rules they depend on.

As explained in Appendix B, the calculations of tensors  $\beta^{eem}$ ,  $\beta^{eme}$ ,  $\beta^{mee}$ ,  $\beta^{eeQ}$ ,  $\beta^{eQe}$  and  $\beta^{Qee}$  follow from Eq. (3) after elementary substitutions of one electric dipole transition moment by one magnetic dipole moment or one electric quadrupole moment, respectively, according to the appropriate light-matter Hamiltonians. Calculations of the generic terms of  $\beta^{eem}$  and  $\beta^{Qee}$  are provided as examples in Appendix B.

The formal definition of all these elementary response functions in terms of electric fields, their gradients and magnetic fields is local at the microscopic level. In order to apply these response functions to actual experimental data analysis, we still have to relate them to measurable input and output quantities, i.e. intensities proportional to the squared amplitudes of the electric far fields. They are equal to the local fields in vacuum, but not in condensed media. As for the right-hand sides of Eqs. (4–6), local electric fields are known to relate to their far field counterparts through Fresnel factors,<sup>4,54,55</sup> and electric field gradients follow accordingly.<sup>56</sup> As for the local magnetic fields, appropriate modified

Fresnel factors (Appendix C) also relate them to the far electric fields,<sup>57</sup> provided that a plane wave description is assumed as is the case in the second quantization formalism of the electromagnetic field.<sup>39</sup> The emitted SFG intensity originates from the three sources listed at the left-hand sides of Eqs. (4–6). For a single emitter, the emitted SFG field arises from the multipole expansion of the scattered field in the radiation zone, as accounted for by the textbooks.<sup>16,58</sup> Usually, as far as SFG experiments are concerned, an assembly of emitters is considered, building up a macroscopic medium described by its volume (or surface) densities of sources, namely electric polarization  $\mathbf{P}(\mathbf{r})$ , magnetic polarization  $\mathbf{M}(\mathbf{r})$  and electric quadrupole moment density  $\mathbf{Q}(\mathbf{r})$ , by averaging the microscopic sources over a unit volume. Although specific Fresnel factors may be calculated to relate these electric,<sup>4,59</sup> magnetic<sup>57</sup> (Appendix C) and quadrupolar source densities to the emitted far electric field, the easiest method consists in embedding them into an effective dipole source<sup>15,17</sup>  $\mathbf{P}_{\text{eff}}(\mathbf{r})$  before calculating the emitted field:

$$\mathbf{P}_{\text{eff}}(\omega_3, \mathbf{r}) = \mathbf{P}(\omega_3, \mathbf{r}) - \frac{1}{2} \overset{t}{\nabla} \mathbf{Q}(\omega_3, \mathbf{r}) + \frac{\imath}{\omega_3} \nabla \times \mathbf{M}(\omega_3, \mathbf{r}), \quad (7)$$

where the last term is obtained by assuming the time harmonicity of the fields.

### III. BIPARTITE SYSTEMS

When the system is composed of two subunits, the full response functions of the system have to take into account the capabilities of the two units to exchange energy as part of the response process. This energy exchange is parametrized by an interaction Hamiltonian and graphically represented in the diagrams by the exchange of a real (or virtual, possibly) vector boson (Fig. 2). The response functions without energy exchange,  $\boldsymbol{\alpha}^{[0]}$  and  $\boldsymbol{\beta}^{[0]}$ , may be seen as the zeroth-order response in terms of interaction Hamiltonian. Still, the higher order terms involving energy exchange may dominate the response, as is well-known for a molecule-nanoparticle system under the electric dipole approximation: the (eee) molecular SFG response function indeed involves first-order terms driven by the nanoparticle polarizability, which becomes giant when the beam energy matches the surface plasmon resonance energy.<sup>9,12,14</sup>

Below, we consider the SFG response function of the molecule and the way it is modi-

fied by the presence of a partner when the whole system is excited by two light beams at frequencies  $\omega_1$  and  $\omega_2$ , generating a third beam at frequency  $\omega_3 = \omega_1 + \omega_2$ . As we have seen in Section II, beyond the electric dipole approximation, this response also encompasses magnetic and quadrupole vertices. This means that we also have to take into account the magnetic and quadrupolar contributions to the interaction Hamiltonian, and the associated bosons. Given that these terms actually represent higher order contributions (i.e. with a smaller order of magnitude) with respect to the electric dipole, we may limit our description to diagrams involving one of such interaction bosons at most. As a consequence of the input and output properties of optical response functions (Feynman rule #1)<sup>11</sup> and of the uniqueness of the SFG vertex (where relationship  $\omega_3 = \omega_1 + \omega_2$  applies, Feynman rule #5),<sup>11</sup> the vector boson energies  $\omega_b$  have to match one of the energies present in the system (i.e.  $\omega_b = \omega_1, \omega_2$  or  $\omega_3$ ), which simplifies the frequency filling of the two-loop diagrams.<sup>12</sup> For magnetic couplings in particular, it is worth noting that the energies linked to a direct interaction between orbital or spin magnetic moments of the molecule and its partner lie far below the accessible optical frequencies at stake in an SFG process. Vector bosons carrying energy in the optical range are actually rather linked to interaction Hamiltonians involving electromagnetic fields (and their gradients) oscillating at optical frequencies. In the following, we restrict our analysis to such electromagnetic Hamiltonians. We do not include the special case of static fields (i.e. involving a zero-frequency boson), which deserves a special treatment in the future: it indeed offers additional perspectives for the interaction between molecules and charged entities (e.g. electrodes) or to account for spin-spin interactions in response to applied magnetic fields (e.g. when ferromagnetic materials or paramagnetic molecules are involved).

## A. Interaction Hamiltonians

In Ref. 11, we have seen that any matter-matter interaction between the subsystems is described in the multipartite loop diagrams by four-particle vertices associated to the canonical interaction Hamiltonian:

$$\mathcal{H}_{\text{int}} = \sum_{a,b} \sum_{m,n} C_{ab,mn} c_m^\dagger d_a^\dagger c_n d_b, \quad (8)$$

where  $\{a, b, d_a^\dagger, d_b\}$  and  $\{m, n, c_m^\dagger, d_n\}$  are the quantum states and the associated fermionic creation/annihilation operators of subsystems 1 and 2, respectively, and  $C_{ab,mn}$  is the coupling constant. Four-particle vertices are conveniently replaced in the diagrams by two three-particle vertices linked by the exchange of a vector boson. As an example, exchange of energy  $\hbar\omega$  through electric dipolar coupling is mediated by the coupling constant

$$C_{ab,mn}^{\text{ee}} = \sum_{h,l} p_{ab}^l W_{lh}^{\text{ee}}(\omega, \mathbf{R}) p_{mn}^h \quad (9)$$

where  $p_{ab}^l$  (resp.  $p_{mn}^h$ ) is the electric dipole transition moment along coordinate  $l$  (resp.  $h$ ) between states  $b$  and  $a$  (resp.  $n$  and  $m$ ) for subsystem 1 (resp. subsystem 2), and  $\mathbf{R} = \mathbf{r}_1 - \mathbf{r}_2$  is the relative position of the subsystems. The matrix  $\mathbf{W}^{\text{ee}}$  is classically given by:<sup>12,16,39</sup>

$$W_{lh}^{\text{ee}}(\omega, \mathbf{R}) = \frac{e^{i\omega|\mathbf{R}|/c}}{4\pi\epsilon_0|\mathbf{R}|^3} \left[ \delta_{lh} \left( 1 - i\frac{\omega|\mathbf{R}|}{c} - \frac{\omega^2|\mathbf{R}|^2}{c^2} \right) - \hat{R}_l \hat{R}_h \left( 3 - 3i\frac{\omega|\mathbf{R}|}{c} - \frac{\omega^2|\mathbf{R}|^2}{c^2} \right) \right], \quad (10)$$

where  $\hat{\mathbf{R}} = \mathbf{R}/|\mathbf{R}|$ . In Eq. (9), the full coupling constant is thus decomposed into a coupling constant  $p_{mn}^h$  between subsystem 2 and the boson, a boson propagator  $W_{lh}^{\text{ee}}$  (with energy  $\hbar\omega$  flowing from  $h$  at subsystem 2 to  $l$  at subsystem 1), and a coupling constant  $p_{ab}^l$  between the boson and subsystem 1. Eq. (9) can be seen as the projection onto states  $\{a, b, m, n\}$  of the classical interaction energy evaluated at subsystem 1:

$$\langle \mathcal{H}_{\text{int}}^{\text{ee}} \rangle = -\mathbf{p}_1 \cdot \mathbf{E}_2(\omega, \mathbf{R}), \quad (11)$$

where  $\mathbf{p}_1$  is the dipole moment of subsystem 1 and  $\mathbf{E}_2(\omega, \mathbf{R}) = -\mathbf{W}^{\text{ee}}(\omega, \mathbf{R}) \mathbf{p}_2$  is the electric field created at subsystem 1 by the dipole moment  $\mathbf{p}_2$  of subsystem 2.

The nature of the coupling process at each interaction vertex influences both the value of the boson propagator and the nature of the loop in which the vertex is embedded. From the description of elementary response functions in Section II, we see that it is possible to involve magnetic dipole and quadrupole vertices in multipartite diagrams provided that the boson propagator is adapted accordingly. We separate magnetic from quadrupolar contributions and avoid cross contributions between them.

## 1. Quadrupolar interactions

For matter-matter quadrupolar interactions, we only consider vertices implying one quadrupole moment and we thus discard the case of quadrupole-quadrupole interactions. The first (Qe) coupling constant we are interested in is then defined as:

$$C_{ab,mn}^{\text{Qe}} = \sum_{h,l,\zeta} q_{ab}^{\zeta l} W_{\zeta lh}^{\text{Qe}}(\omega, \mathbf{R}) p_{mn}^h, \quad (12)$$

and classically driven by:

$$\langle \mathcal{H}_{\text{int}}^{\text{Qe}} \rangle = -\frac{1}{2} (\mathbf{q}_1 \nabla) \cdot \mathbf{E}_2(\omega, \mathbf{R}). \quad (13)$$

As the dipolar electric field created by subsystem 2 reads  $\mathbf{E}_2 = -\mathbf{W}^{\text{ee}} \mathbf{p}_2$ , we get:

$$\langle \mathcal{H}_{\text{int}}^{\text{Qe}} \rangle = -\frac{1}{2} \sum_{\zeta,l} q_1^{\zeta l} \partial_{\zeta} E_2^l(\omega, \mathbf{R}) = \frac{1}{2} \sum_{\zeta,l,h} q_1^{\zeta l} \partial_{\zeta} W_{lh}^{\text{ee}}(\omega, \mathbf{R}) p_2^h. \quad (14)$$

We deduce that:

$$W_{\zeta lh}^{\text{Qe}}(\omega, \mathbf{R}) = \frac{1}{2} \partial_{\zeta} W_{lh}^{\text{ee}}(\omega, \mathbf{R}). \quad (15)$$

By derivating the expression of  $\mathbf{W}^{\text{ee}}$  given by Eq. (10), we show that:

$$W_{\zeta lh}^{\text{Qe}}(\omega, \mathbf{R}) = \frac{e^{i\omega|\mathbf{R}|/c}}{8\pi\epsilon_0|\mathbf{R}|^4} \left[ \hat{R}_{\zeta} \delta_{lh} \left( -3 + 3i \frac{\omega|\mathbf{R}|}{c} + 2 \frac{\omega^2|\mathbf{R}|^2}{c^2} - i \frac{\omega^3|\mathbf{R}|^3}{c^3} \right) \right. \quad (16)$$

$$\left. + \hat{R}_{\zeta} \hat{R}_l \hat{R}_h \left( 15 - 15i \frac{\omega|\mathbf{R}|}{c} - 6 \frac{\omega^2|\mathbf{R}|^2}{c^2} + i \frac{\omega^3|\mathbf{R}|^3}{c^3} \right) \right. \quad (17)$$

$$\left. + (\delta_{\zeta h} \hat{R}_l + \delta_{\zeta l} \hat{R}_h) \left( -3 + 3i \frac{\omega|\mathbf{R}|}{c} + \frac{\omega^2|\mathbf{R}|^2}{c^2} \right) \right]. \quad (18)$$

As for the (eQ) coupling constant, the  $\mathbf{W}^{\text{eQ}}$  tensor is defined by:

$$C_{ab,mn}^{\text{eQ}} = \sum_{h,l,\zeta} p_{ab}^l W_{l\zeta h}^{\text{eQ}}(\omega, \mathbf{R}) q_{mn}^{\zeta h}. \quad (19)$$

Assuming the (eQ/Qe) symmetry of the dipole-quadrupole interaction leads to  $C_{ab,mn}^{\text{eQ}} = C_{mn,ab}^{\text{Qe}}$  and enables us to write:

$$p_{ab}^l W_{l\zeta h}^{\text{eQ}} q_{mn}^{\zeta h} = q_{mn}^{\zeta l} W_{\zeta lh}^{\text{Qe}} p_{ab}^h = p_{ab}^l W_{\zeta hl}^{\text{Qe}} q_{mn}^{\zeta h} = p_{ab}^l W_{\zeta hl}^{\text{Qe}} q_{mn}^{h\zeta} = p_{ab}^l W_{h\zeta l}^{\text{Qe}} q_{mn}^{\zeta h}, \quad (20)$$

where the summation is implicit for all pairs of identical indices/superscripts. In Eq. (20), the second equality is obtained through the permutation of the dummy indices  $l$  and  $h$ , the third one is based on the transposition symmetry of  $\mathbf{q}$ , and the fourth one follows from the permutation of the dummy indices  $h$  and  $\zeta$ . As the  $\mathbf{W}^{\text{Qe}}$  tensor is invariant under the permutation of its last two indices, we eventually get:

$$W_{l\zeta h}^{\text{eQ}} = W_{hl\zeta}^{\text{Qe}}. \quad (21)$$

This expression of the propagator  $W_{l\zeta h}^{\text{eQ}}$ , as deduced from Eq. (16–18), coincides with that of the quadrupolar Green's tensor  $\mathbf{G}^{\text{Q}}$  computed by A. B. Evlyukhin *et al.*, which relates the moment  $\mathbf{q}$  to the electric field  $\mathbf{E}^{\text{Q}}$  it creates<sup>50,60</sup> [see Eqs. (7) and (23) in these two references, respectively]:

$$E_l^{\text{Q}}(\omega, \mathbf{R}) = - \sum_{l, \zeta} W_{h\zeta h}^{\text{eQ}}(\omega, \mathbf{R}) q_{\zeta h} = - \frac{\omega^2}{\varepsilon_0 c^2} \sum_{h, \zeta} G_{l\zeta}^{\text{Q}}(\omega, \mathbf{R}) \hat{R}_h q'_{\zeta h}. \quad (22)$$

where  $\mathbf{q}' = 3\mathbf{q} - (\text{Tr } \mathbf{q})\mathbf{1}$  is the traceless definition of the quadrupole moment. The demonstration of Eq. (22) is derived in Appendix D.

## 2. Magnetic interactions

For matter-matter magnetic interactions, we have three coupling constants to consider: two electric-magnetic (em/me) vertices, and one purely magnetic (mm) vertex. The first (me) interaction tensor  $\mathbf{W}^{\text{me}}$  is defined with respect to the coupling constant:

$$C_{ab, mn}^{\text{me}} = \sum_{h, l} \mu_{ab}^l W_{lh}^{\text{me}}(\omega, \mathbf{R}) p_{mn}^h, \quad (23)$$

corresponding to the classical interaction energy:

$$\langle \mathcal{H}_{\text{int}}^{\text{me}} \rangle = -\boldsymbol{\mu}_1 \cdot \mathbf{B}_2(\omega, \mathbf{R}), \quad (24)$$

where  $\mathbf{B}_2$  is the magnetic field created at point  $\mathbf{R}$  by the electric dipole  $\mathbf{p}_2$ . From the Maxwell-Faraday equation expressed in time harmonic regime,  $i\omega \mathbf{B}_2 = \nabla \times \mathbf{E}_2 = -\nabla \times (\mathbf{W}^{\text{ee}} \mathbf{p}_2)$ .

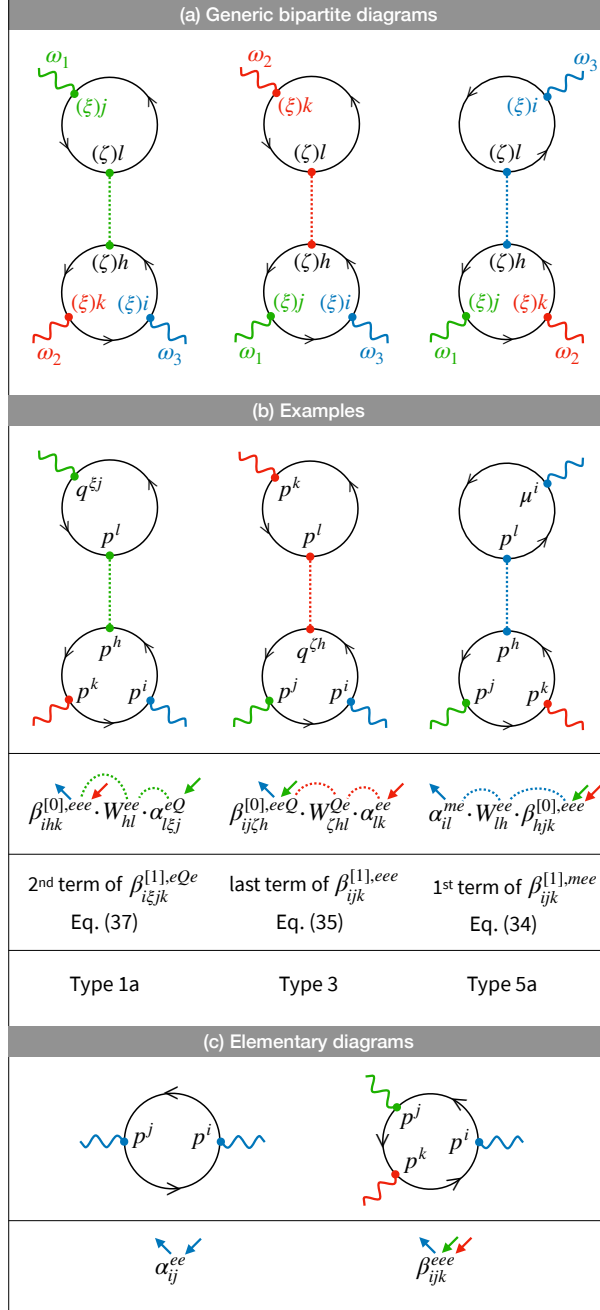


FIG. 2. (a) Generic bipartite diagrams. (b) Examples of Type 1a, 3 and 5a diagrams (see Table I). The second line illustrates how to interpret each diagram (from right to left). (c) Reminder of the elementary diagrams (at pure electric dipole level), given for comparison.

As a result:

$$\langle \mathcal{H}_{\text{int}}^{\text{me}} \rangle = \frac{1}{i\omega} \sum_{l,k,h,\zeta} \mu_1^l \epsilon_{l\zeta k} \partial_\zeta W_{kh}^{\text{ee}} p_2^h, \quad (25)$$

where  $\epsilon = (\epsilon_{ijk})$  is the Levi-Civita tensor. Henceforth, we identify:

$$W_{lh}^{\text{me}}(\omega, \mathbf{R}) = \frac{1}{i\omega} \sum_{k,\zeta} \epsilon_{l\zeta k} \partial_{\zeta} W_{kh}^{\text{ee}}(\omega, \mathbf{R}) = \frac{2}{i\omega} \sum_{k,\zeta} \epsilon_{l\zeta k} W_{\zeta kh}^{\text{Qe}}(\omega, \mathbf{R}). \quad (26)$$

From Eq. (15), the (me) coupling matrix indeed turns out to be a tensor contraction between  $\epsilon$  and  $\mathbf{W}^{\text{Qe}}$ . Thanks to Eq. (16–18), we find:

$$W_{lh}^{\text{me}}(\omega, \mathbf{R}) = \frac{e^{i\omega|\mathbf{R}|/c}}{4\pi\epsilon_0|\mathbf{R}|^4} \frac{1}{i\omega} \sum_{\zeta,k} \epsilon_{l\zeta k} \hat{R}_{\zeta} \delta_{kh} \left( -3 + 3i\frac{\omega|\mathbf{R}|}{c} + 2\frac{\omega^2|\mathbf{R}|^2}{c^2} - i\frac{\omega^3|\mathbf{R}|^3}{c^3} \right) + \epsilon_{l\zeta k} \hat{R}_k \delta_{\zeta h} \left( -3 + 3i\frac{\omega|\mathbf{R}|}{c} + \frac{\omega^2|\mathbf{R}|^2}{c^2} \right). \quad (27)$$

Note that the Levi-Civita tensor removes the symmetric terms of  $W_{\zeta kh}^{\text{Qe}}$  with respect to the first two indices. Through permutations of dummy indices, we eventually get:

$$W_{lh}^{\text{me}}(\omega, \mathbf{R}) = \frac{e^{i\omega|\mathbf{R}|/c}}{4\pi\epsilon_0c|\mathbf{R}|^3} \left( i\frac{\omega|\mathbf{R}|}{c} + \frac{\omega^2|\mathbf{R}|^2}{c^2} \right) \sum_k \epsilon_{lhk} \hat{R}_k \quad (28)$$

This result coincides with the Eqs. (21) and (11) in Refs. 60 and 61, respectively. In the same way, the (em) interaction is driven by:

$$\mathcal{H}_{\text{int}}^{\text{em}} = -\mathbf{p}_1 \cdot \mathbf{E}_2(\omega, \mathbf{R}), \quad (29)$$

where the electric field is created by a magnetic dipole set at subsystem 2. We have:<sup>58</sup>

$$\mathcal{H}_{\text{int}}^{\text{em}} = -\frac{e^{i\omega|\mathbf{R}|/c}}{4\pi\epsilon_0c|\mathbf{R}|^3} \left( i\frac{\omega|\mathbf{R}|}{c} + \frac{\omega^2|\mathbf{R}|^2}{c^2} \right) \mathbf{p}_1 \cdot (\boldsymbol{\mu}_2 \times \hat{\mathbf{R}}), \quad (30)$$

leading to the coupling constant  $C_{ab,mn}^{\text{em}} = \sum_{h,l} p_{ab}^l W_{lh}^{\text{em}}(\omega, \mathbf{R}) \mu_{mn}^h$  driven by:

$$W_{lh}^{\text{em}}(\omega, \mathbf{R}) = -\frac{e^{i\omega|\mathbf{R}|/c}}{4\pi\epsilon_0c|\mathbf{R}|^3} \left( i\frac{\omega|\mathbf{R}|}{c} + \frac{\omega^2|\mathbf{R}|^2}{c^2} \right) \sum_k \epsilon_{lhk} \hat{R}_k. \quad (31)$$

We see that  $W_{lh}^{\text{em}} = -W_{lh}^{\text{me}} = W_{hl}^{\text{me}}$  (as  $\epsilon_{ijk} = -\epsilon_{ikj}$ ), which restores the expected symmetry between  $C^{\text{em}}$  and  $C^{\text{me}}$  when subsystems 1 and 2 are swapped. In addition, these terms have no static contributions, i.e. they tend to zero for small distances between the partners (when

$\omega|\mathbf{R}|/c \ll 1$ ).

Finally, it is interesting to consider the magnetic dipole-dipole interaction. The equations describing the magnetic field emitted by a magnetic dipole and the electric field emitted by an electric dipole being symmetric, we directly get:

$$W_{lh}^{\text{mm}}(\omega, \mathbf{R}) = \frac{1}{c^2} W_{lh}^{\text{ee}}(\omega, \mathbf{R}). \quad (32)$$

This defines the (mm) coupling constant:

$$C_{ab,mn}^{\text{mm}} = \sum_{h,l} \mu_{ab}^l W_{lh}^{\text{mm}}(\omega, \mathbf{R}) \mu_{mn}^h. \quad (33)$$

## B. Bipartite diagrams

Bipartite diagrams are constructed and calculated according to the Feynman rules defined previously.<sup>11</sup> Each subsystem is represented by a distinct loop, which may interact with one or several photons involved in the SFG process. As the magnetic and quadrupolar contributions are higher order effects in comparison with the electric dipole terms, we limit the enumeration of diagrams to those which only involve the exchange of one vector boson. In addition, as we are interested in the molecular SFG response in the presence of a partner, (i) the lower loop is ascribed to the ‘molecule’ and the upper loop to its ‘partner’, which may span many natures (nanostructure, fellow molecule, substrate, surface charges, etc.), and (ii) we set the nonlinear vertex (where the constitutive relationship  $\omega_3 = \omega_1 + \omega_2$  actually takes place) on the molecular loop. As a consequence of these considerations, the molecular loop has three interaction vertices (two photons and the vector boson), whereas the partner loop exhibits two vertices (one photon and the vector boson).

The three generic bipartite diagrams are shown in Fig. 2. The full list of allowed diagrams is obtained by: (i) applying full permutations of light-matter vertices  $i$ ,  $j$  and  $k$  over the two loops; (ii) defining the natures (electric dipole, magnetic dipole, quadrupole) of light-matter interactions at these vertices; and (iii) defining the nature of the vector boson (i.e. matter-matter interaction). In principle, each kind of interaction (electric, magnetic or quadrupolar) may happen at each vertex, under a light-matter or matter-matter form. This is represented in Fig. 2, wherein we label light-matter vertices with  $(\xi)v$  and matter-matter vertices with

( $\zeta$ ) $u$ , so that single indexes  $v$  and  $u$  stand for an electric (via  $p^v$  and  $p^u$ ) or a magnetic (via  $\mu^v$  and  $\mu^u$ ) interaction vertex, and double indexes  $\xi v$  and  $\zeta u$  for a quadrupolar vertex (via  $q^{\xi v}$  or  $q^{\zeta u}$ ) encompassing the operator  $\partial_\xi$  or  $\partial_\zeta$ . This leads to very big amounts of diagrams<sup>43</sup> but, owing to selections rules based on the symmetry properties of the different  $\alpha$  and  $\beta$  response functions and the perturbative orders of magnetic and quadrupolar terms, it is possible to reduce the number of relevant diagrams. As explained in details in section IV, a bipartite diagram is discarded if one of these three conditions is satisfied: (i) it contains both magnetic and quadrupolar vertices, (ii) it is built with a (QQ) matter-matter vertex, or (iii) its molecular loop exhibits more than one non-electric dipolar vertex.

While  $\beta^{[0]}$  depicts the hyperpolarizability of the molecule without interaction with the partner, the calculation of the one-boson bipartite diagrams leads to a partner-modified hyperpolarizability  $\beta^{[1]}$  and enables to compute the total molecular response  $\beta$  of the composite system as  $\beta = \beta^{[0]} + \beta^{[1]}$ . This approach follows the same path as was done previously for all-electric dipole diagrams involving only one boson.<sup>11,12</sup> In a general way, the unperturbed molecular hyperpolarizability  $\beta^{[0]}$  is modified by the presence of the partner when one of the three beams (incoming or emitted) interacts with the partner (through one of its polarizabilities  $\alpha$ ) and is conveyed to the molecule (by the boson propagator  $\mathbf{W}$ ) where the nonlinear SFG process takes place. Here, the result is complicated by the higher rank of the tensors describing the elementary building blocks  $\beta^{[0]}$ ,  $\mathbf{W}$  and  $\alpha$  when they involve quadrupolar vertices. For diagrams involving only dipolar vertices (i.e. only electric and magnetic dipoles), the resulting  $\beta^{[1]}$  may be represented by the generic formula:

$$\begin{aligned}
-\beta_{ijk}^{[1]}(\omega_1, \omega_2) &= \alpha_{il}(\omega_3)W_{lh}(\omega_3)\beta_{hjk}^{[0]}(\omega_1, \omega_2) \\
&+ \beta_{ihk}^{[0]}(\omega_1, \omega_2)W_{hl}(\omega_1)\alpha_{lj}(\omega_1) \\
&+ \beta_{ijh}^{[0]}(\omega_1, \omega_2)W_{hl}(\omega_2)\alpha_{lk}(\omega_2),
\end{aligned} \tag{34}$$

where the summation over the  $\{l, h\}$  indices of  $\mathbf{W}$  is implicit. As pictured in Fig. 2, each term may be straightforwardly read from right to left in order to follow the energy flux and the logical sequence of each process. Explicitly, in the first term of Eq. (34), the incoming beams interact with the molecule (through  $\beta^{[0]}$ ) to create a dipole (electric or magnetic) oscillating at frequency  $\omega_3$ . Its energy  $\hbar\omega_3$  is conveyed to the partner (by  $\mathbf{W}$ ) where it is converted (through  $\alpha$ ) into the response dipole, hence encoded by the output of  $\beta^{[1]}$ . In

the second term, the incoming photon at frequency  $\omega_1$  interacts with the partner (through  $\alpha$ ) to generate an oscillating dipole which energy is conveyed to the molecule (by  $\mathbf{W}$ ) in order to take part in the SFG process (through  $\beta^{[0]}$ ) and produce the output dipole. Fixing the natures of  $\beta^{[0]}$  [i.e. (eee), (eem), (eme) or (mee)] and  $\alpha$  [i.e. (ee), (em), (me) or (mm)] unequivocally determines those of  $\mathbf{W}$ ,  $\beta^{[1]}$  and the output dipole.

Type	$\alpha$	$\mathbf{W}$	$\beta^{[0]}$	$\mathbf{W}$	$\alpha$	Vector boson	Q/m vertex	$\beta^{[1]}$
1a	—	—	eee	ee	eQ	$\omega_1, \omega_2$	$\omega_1, \omega_2$	eQe, eeQ
	Qe	ee	eee	—	—	$\omega_3$	$\omega_3$	Qee
1b	—	—	eee	eQ	QQ	$\omega_1, \omega_2$	$\omega_1, \omega_2$	eQe, eeQ
	QQ	Qe	eee	—	—	$\omega_3$	$\omega_3$	Qee
2	—	—	eee	eQ	Qe	$\omega_1, \omega_2$	$\omega_1, \omega_2$	eee
	eQ	Qe	eee	—	—	$\omega_3$	$\omega_3$	eee
3	—	—	eQe, eeQ	Qe	ee	$\omega_1, \omega_2$	$\omega_1, \omega_2$	eee
	ee	eQ	Qee	—	—	$\omega_3$	$\omega_3$	eee
4	—	—	eQe, eeQ	ee	ee	$\omega_2, \omega_1$	$\omega_1, \omega_2$	eQe, eeQ
	ee	ee	eQe, eeQ	—	—	$\omega_3$	$\omega_1, \omega_2$	eQe, eeQ
	—	—	Qee	ee	ee	$\omega_1, \omega_2$	$\omega_3$	Qee
5a	—	—	eee	ee	em	$\omega_1, \omega_2$	$\omega_1, \omega_2$	eme, eem
	me	ee	eee	—	—	$\omega_3$	$\omega_3$	mee
5b	—	—	eee	em	mm	$\omega_1, \omega_2$	$\omega_1, \omega_2$	eme, eem
	mm	me	eee	—	—	$\omega_3$	$\omega_3$	mee
6	—	—	eee	em	me	$\omega_1, \omega_2$	$\omega_1, \omega_2$	eee
	em	me	eee	—	—	$\omega_3$	$\omega_3$	eee
7a	—	—	eme, eem	me	ee	$\omega_1, \omega_2$	$\omega_1, \omega_2$	eee
	ee	em	mee	—	—	$\omega_3$	$\omega_3$	eee
7b	—	—	eme, eem	mm	me	$\omega_1, \omega_2$	$\omega_1, \omega_2$	eee
	em	mm	mee	—	—	$\omega_3$	$\omega_3$	eee
8	—	—	eme, eem	ee	ee	$\omega_2, \omega_1$	$\omega_1, \omega_2$	eme, eem
	ee	ee	eme, eem	—	—	$\omega_3$	$\omega_1, \omega_2$	eme, eem
	—	—	mee	ee	ee	$\omega_1, \omega_2$	$\omega_3$	mee

TABLE I. List of composite SFG response functions ( $\beta^{[1]}$ ) of the molecule-partner system involving ‘Q’ [Eqs. (35-38)] or ‘m’ [Eq. (34)] vertices. The ‘vector boson’ column gives the frequency that is conveyed by the matter-matter vertex (via  $\mathbf{W}$ ) and goes through the partner (via  $\alpha$ ), following a logical sequence to be read from right to left as explained in the text. The ‘Q/m vertex’ column indicates which photon frequency is assigned to the quadrupolar or magnetic vertex implied in the process. Each ‘type’ of diagram is defined by the respective (e/m/Q) natures of  $\beta^{[1]}$  and  $\beta^{[0]}$ .

When quadrupolar interaction is introduced instead, a new set of terms appears:

$$\begin{aligned}
-\beta_{ijk}^{[1],eee}(\omega_1, \omega_2) &= \alpha_{i\zeta l}^{eQ}(\omega_3)W_{\zeta lh}^{Qe}(\omega_3)\beta_{hjk}^{[0],eee}(\omega_1, \omega_2) + \alpha_{il}^{ee}(\omega_3)W_{l\zeta h}^{eQ}(\omega_3)\beta_{\zeta hjk}^{[0],Qee}(\omega_1, \omega_2) \\
&+ \beta_{ihk}^{[0],eee}(\omega_1, \omega_2)W_{h\zeta l}^{eQ}(\omega_1)\alpha_{\zeta lj}^{Qe}(\omega_1) + \beta_{i\zeta hk}^{[0],eQe}(\omega_1, \omega_2)W_{\zeta hl}^{Qe}(\omega_1)\alpha_{lj}^{ee}(\omega_1) \\
&+ \beta_{ijh}^{[0],eee}(\omega_1, \omega_2)W_{h\zeta l}^{eQ}(\omega_2)\alpha_{\zeta lk}^{Qe}(\omega_2) + \beta_{ij\zeta h}^{[0],eeQ}(\omega_1, \omega_2)W_{\zeta hl}^{Qe}(\omega_2)\alpha_{lk}^{ee}(\omega_2), \quad (35)
\end{aligned}$$

$$\begin{aligned}
-\beta_{\xi jk}^{[1],Qee}(\omega_1, \omega_2) &= \alpha_{\xi il}^{Qe}(\omega_3)W_{lh}^{ee}(\omega_3)\beta_{hjk}^{[0],eee}(\omega_1, \omega_2) \\
&+ \beta_{\xi i hk}^{[0],Qee}(\omega_1, \omega_2)W_{hl}^{ee}(\omega_1)\alpha_{lj}^{ee}(\omega_1) \\
&+ \beta_{\xi ijh}^{[0],Qee}(\omega_1, \omega_2)W_{hl}^{ee}(\omega_2)\alpha_{lk}^{ee}(\omega_2) \\
&+ \alpha_{\xi i\zeta l}^{QQ}(\omega_3)W_{\zeta lh}^{Qe}(\omega_3)\beta_{hjk}^{[0],eee}(\omega_1, \omega_2), \quad (36)
\end{aligned}$$

$$\begin{aligned}
-\beta_{i\xi jk}^{[1],eQe}(\omega_1, \omega_2) &= \alpha_{il}^{ee}(\omega_3)W_{lh}^{ee}(\omega_3)\beta_{h\xi jk}^{[0],eQe}(\omega_1, \omega_2) \\
&+ \beta_{ihk}^{[0],eee}(\omega_1, \omega_2)W_{hl}^{ee}(\omega_1)\alpha_{l\xi j}^{eQ}(\omega_1) \\
&+ \beta_{i\xi jh}^{[0],eQe}(\omega_1, \omega_2)W_{hl}^{ee}(\omega_2)\alpha_{lk}^{ee}(\omega_2) \\
&+ \beta_{ihk}^{[0],eee}(\omega_1, \omega_2)W_{h\zeta l}^{eQ}(\omega_1)\alpha_{\zeta l\xi j}^{QQ}(\omega_1), \quad (37)
\end{aligned}$$

$$\begin{aligned}
-\beta_{ij\xi k}^{[1],eeQ}(\omega_1, \omega_2) &= \alpha_{il}^{ee}(\omega_3)W_{lh}^{ee}(\omega_3)\beta_{hj\xi k}^{[0],eeQ}(\omega_1, \omega_2) \\
&+ \beta_{ih\xi k}^{[0],eeQ}(\omega_1, \omega_2)W_{hl}^{ee}(\omega_1)\alpha_{lj}^{ee}(\omega_1) \\
&+ \beta_{ijh}^{[0],eee}(\omega_1, \omega_2)W_{hl}^{ee}(\omega_2)\alpha_{l\xi k}^{eQ}(\omega_2) \\
&+ \beta_{ijh}^{[0],eee}(\omega_1, \omega_2)W_{h\zeta l}^{eQ}(\omega_2)\alpha_{\zeta l\xi k}^{QQ}(\omega_2), \quad (38)
\end{aligned}$$

where implicit summations over redundant indices (i.e. those of  $\mathbf{W}$ ) apply for each term. The different types of composite diagrams are summarized in Table I for both quadrupolar and magnetic contributions.

## IV. CONSEQUENCES OF SYMMETRY AND GEOMETRY

### A. Symmetries of uncoupled objects

Before considering bipartite systems, we first recall the influence of the symmetry properties of (i) any individual object at the microscopic scale and (ii) a macroscopic collection of such objects on their linear and nonlinear optical response functions. Indeed, second-order nonlinear optical processes like SFG have gained interest as they are symmetry-driven, in particular with respect to inversion symmetry: the first hyperpolarizability  $\beta^{[0],eee}$  of a single centrosymmetric object vanishes at the electric dipole level of theory. In addition, at the macroscopic scale, the second-order susceptibility  $\chi^{(2)}$  is obtained by summing up all individual hyperpolarizability contributions over a unit volume, taking into account the orientation average of the individual objects through  $\chi^{(2)} = N\langle\beta^{[0],eee}\rangle$ , where  $N$  is their volume density. Even for non-centrosymmetric objects (i.e.  $\beta^{[0],eee} \neq 0$ ), isotropic averaging cancels  $\chi^{(2)}$  when it gives rise to a ‘‘centrosymmetric bulk’’ (e.g. when objects are embedded as a solute in a liquid phase), thus no phase-matched SFG is produced. SFG may still alternatively be measured in this case in the scattering geometry,<sup>62,63</sup> provided that the individual objects are big enough as compared to the wavelengths of light. It is also worth noting that the isotropic distribution of chiral entities is not centrosymmetric,<sup>64–66</sup> leaving open the possibility to measure a dipolar contribution from the bulk.<sup>67</sup> This is actually the only situation giving rise to coherent SFG production from an isotropic bulk in the electric dipole approximation.<sup>68</sup>

In Part II, we have defined new response functions beyond the electric dipolar level. It is in fact rather easy to establish, by direct inspection<sup>69</sup> or by writing down the transformations of the various quantities,<sup>45</sup> the behaviors of the various  $\alpha$  and  $\beta$  tensors upon inversion symmetry  $C_i$ . Some of them vanish indeed and are marked as such in Table II. We note in particular that only  $\beta^{[0],eee}$  vanishes for a centrosymmetric molecule, while hybrid  $\alpha^{eQ/Qe}$  and  $\alpha^{em/me}$  do vanish for a centrosymmetric partner. The same conclusions apply to their macroscopic counterparts describing a centrosymmetric bulk. In other words, for a centrosymmetric single object or distribution of objects, only the (ee) contribution to linear optics survives at first order in ‘m’ and ‘Q’ vertices, whereas the (eee) term is the only one to vanish for SFG: all the other contributions in Eqs. (34–38) are allowed by symmetry.

Type	$\beta^{[1]}$		$\beta^{[0]}$		$\mathbf{W}$	$\boldsymbol{\alpha}$	
	Nature	$C_i ?$	Nature	$C_i ?$	Nature	Nature	$C_i ?$
0	eee	NO	eee	NO	ee	ee	YES
1a	Qee/eQe/eeQ	YES	eee	NO	ee	eQ/Qe	NO
1b	Qee/eQe/eeQ	YES	eee	NO	eQ/Qe	QQ	YES
2	eee	NO	eee	NO	eQ/Qe	eQ/Qe	NO
3	eee	NO	Qee/eQe/eeQ	YES	eQ/Qe	ee	YES
4	Qee/eQe/eeQ	YES	Qee/eQe/eeQ	YES	ee	ee	YES
5a	mee/eme/eem	YES	eee	NO	ee	me/em	NO
5b	mee/eme/eem	YES	eee	NO	me/em	mm	YES
6	eee	NO	eee	NO	me/em	me/em	NO
7a	eee	NO	mee/eme/eem	YES	me/em	ee	YES
7b	eee	NO	mee/eme/eem	YES	mm	me/em	NO
8	mee/eme/eem	YES	mee/eme/eem	YES	ee	ee	YES

TABLE II. Classification of the one-boson SFG response functions  $\beta^{[1]}$  of the molecule-partner system involving one ‘Q’ or ‘m’ vertex, each type being represented by one member. The columns labelled “ $C_i ?$ ” indicate whether each quantity  $\beta$ ,  $\mathbf{W}$  or  $\boldsymbol{\alpha}$  survives under inversion symmetry, i.e. whether the process is allowed for a centrosymmetric entity or an isotropic bulk. The conventional case of purely electric dipolar responses is recalled for information, referred as type 0.

### 1. First-order response of centrosymmetric objects

Considering the typical example of a spherical nanoparticle, its intrinsic contribution to the linear optical phenomena is driven by  $\boldsymbol{\alpha}^{ee}$ , provided its size is negligible with respect to the wavelength of light. It is indeed well-known that big nanospheres exhibit an additional first-order quadrupolar response, as experimentally measured in solution<sup>70</sup> and predicted by the Mie theory.<sup>16,71,72</sup> The associated quadrupolar Mie response, quantified by the so-called  $a_2$  coefficient,<sup>72</sup> derives from an isotropic quadrupolar polarizability consisting in an  $\boldsymbol{\alpha}^{QQ}$  response function,<sup>49,50</sup> actually allowed for centrosymmetric objects (whereas  $\boldsymbol{\alpha}^{eQ/Qe} = \mathbf{0}$ ). In such a case, the (QQ) term represents the first nonvanishing correction to the purely electric dipole contribution and must be included in our analysis (hence type 1b in Table II) in order to take the quadrupolar terms involved in a molecule-nanosphere system into account, for instance. Interestingly, the literature counts other experimental evidences of quadrupolar optical responses in the case non-centrosymmetric nanoparticles deposited on solid substrates, like rings<sup>73</sup> or cylinders.<sup>74</sup> For such in-plane symmetric particles, the (Qe) response has proved to vanish when excited at normal incidence (i.e. along the symmetry axes) because the in-plane isotropy is enforced. Moreover, the (QQ) term is too small to be measured as the sole surface response is generated by a small number of objects. Conversely,

a (Qe) contribution becomes measurable at oblique incidence, for which the breaking of the in-plane isotropy and retardation effects indeed induce a quadrupole.<sup>74,75</sup> For such particles, the (Qe) and (eQ) responses dominate the quadrupolar contribution as long as they are excited away from any in-plane symmetry axis. As a result, it seems reasonable to restrict the use of  $\alpha^{\text{QQ}}$  within bipartite diagrams to the cases of systems involving a spherical partner.

The situation is different for magnetic response functions  $\alpha^{\text{em/me}}$ . They appear in the literature under various forms,<sup>44-48</sup> most of them linked to chiral objects, molecules or nanostructures. As will be discussed later, they quantify the optical activity of molecular systems.<sup>35,36,76</sup> By definition, chiral objects are not centrosymmetric and there is no symmetry reason leading to the vanishing of their  $\alpha^{\text{em/me}}$  tensors. Nevertheless, as for the quadrupolar counterparts, the magnetic contribution to light scattering by a sphere, associated to the  $b_1$  coefficient in the Mie theory, is related to an  $\alpha^{\text{mmm}}$  function.<sup>77</sup> It has been shown to play a role into the coupling of the linear optical response functions of a plasmonic sphere with a dielectric sphere.<sup>61</sup> To account for these specific situations, we also include type-5b diagrams and thus involve  $\alpha^{\text{mmm}}$  response functions in our analysis.

## 2. *Second-order response of centrosymmetric objects*

As mentioned earlier, the situation is opposite for the second-order response functions. For a centrosymmetric object, the (eee) response vanishes whereas, as can be checked in Table II, the  $\beta^{[0]}$  responses involving one ‘m’ or ‘Q’ vertex are allowed. This is in fact well-known for spherical nanoparticles, for which the only contributions to Second-Harmonic Generation (SHG) have been shown to be of the (eeQ), (eQe) and (Qee) types,<sup>20,22</sup> whereas magnetic terms do not contribute because of the presence of mirror planes.<sup>22</sup> Still, (eem), (eme) and (mee) terms should be added when noncollinear and nondegenerate SFG is involved, as is known from the SFG response of a centrosymmetric bulk.<sup>17</sup> Of course, when the (eee) response is also allowed by a lower degree of symmetry, we may expect that it overwhelms these higher order terms. Even so, (eem), (eme) and (mee) terms have been measured in particular cases like thin films of chiral molecules, with orders of magnitude equal to the (eee) contributions when they could be experimentally separated.<sup>78</sup> As for quadrupolar terms, we expect these to significantly contribute when a molecule has a high symmetry,<sup>79</sup> upon dimerization for instance.<sup>19</sup> In these two examples, measurement of size-

able non-dipolar contributions to  $\beta^{[0]}$  may also relate to a possible bulk origin, for which the high number of molecules in the bulk compensates for the low intrinsic values of their  $\beta^{[0]}$ . Conversely, the higher (eee) terms will be limited to the interfaces, with a much lower amount of source molecules.

## B. Geometry of the molecule-partner system

When considering a bipartite system, the situation is complicated by several factors: intrinsic symmetry properties of both the molecule and the partner, orientation averaging of each subunit inside the bipartite system, orientation averaging of their relative positions, relative distance between them and, finally, orientation averaging of the bipartite system as a whole. Here we discuss these different layers of statistical operations.

### 1. *Orientation statistics and symmetries of coupled objects*

The symmetry tables or the methods recalled earlier allow to list the nonvanishing components of the polarizabilities of the partner and the hyperpolarizabilities<sup>68,80,81</sup> of the molecule building up the bipartite system, in the frame of their own symmetry axes. In particular, when one or both are centrosymmetric, the number of allowed processes decreases: only types 3, 4, 7a, 7b and 8 remain for a centrosymmetric molecule, and types 0, 1b, 3, 4, 5b, 7a and 8 for a centrosymmetric partner. For lower symmetries, the analysis of the relevant processes depends on the definition of the system. Starting with one molecule interacting with one partner whose relative positions and orientations are fixed, it is still possible to consider a distribution of such a rigid system in a bulk or at a surface. In this case, an orientation averaging is performed on their total response function  $\beta$  after its calculation. However, this remains rather theoretical and fails most of the times to describe the complexity of actual systems because realistic models must also account for the degrees of freedom (orientation, relative distance) inside the bipartite system. Setting the orientation of the partner in the first place, the molecule may be allowed to move more or less freely around it in short time scales, or adopt several geometric relative conformations with a given probability. This is equivalent to averaging over a distribution of conformations in order to model an average bipartite system in a bulk. In this approach, orientation averaging shall be performed on

the response function of the molecule and/or the coupling constant  $\mathbf{W}$ , depending of the degrees of freedom of the system. Furthermore, when one molecule interacts with several identical partners (e.g. a molecule surrounded by interacting solvent molecules) or when several identical molecules interact with one common partner (e.g. molecules adsorbed at the surface of a nanoparticle), similar averaging operations have to be performed. From ergodicity, averaging over the configuration space of an individual entity is equivalent to averaging over an isotropic spatial distribution of identical entities. Whatever the number of subunits in the system, the complete response function shall then be calculated as a sum over individual response functions, considering that the identical molecules (resp. partners) each adopt a different conformation with respect to the partner (resp. molecule).

As an example, let us consider molecules adsorbed at the surface of a partner nanoparticle, respectively characterized by known  $\beta^{[0]}$  and  $\alpha$  response functions. In order to calculate the molecular SFG response function modified by the presence of the partner, one has to consider that each molecule may adopt several conformations, or an average conformation, for each position at the surface of the particle, leading to different projections of  $\beta^{[0]}$  components onto the local frame of the nanoparticle at this point. Then, a sum over these positions [running more precisely over  $\mathbf{W}(\mathbf{R})$ ] must be performed to scan the particle’s surface and account for the distribution of the molecules around it. Finally, these sums over  $\beta^{[0]}$  and  $\mathbf{W}(\mathbf{R})$  may be coupled or performed sequentially, depending on whether the orientation and distance of the molecule with respect to the partner center depend on its position or not: as an illustration, we can think about the differences between spherical and cubic particles. This may seem like a difficult task, but a straightforward use of the direction cosine matrices<sup>82,83</sup> followed by an integration over the relevant angles and distances provides the expected result, which can be found in the literature for the (eee) response of molecules adsorbed on a spherical nanoparticle, or on a plane located below the particle.<sup>14</sup> As expected, the total nonlinear response of the “molecules on a sphere” system is found to vanish after integration of the molecular individual responses over the whole sphere. Even if the molecular  $\beta^{[0],eee}$  and the nanoparticle  $\alpha^{ee}$  are allowed by symmetry, the total integrated  $\beta$  relates to a multipartite system for which centrosymmetry is recovered, hence its vanishing response as stated in Table II (type 0). This example illustrates a general phenomenon for the symmetry analysis of bipartite systems: not only the symmetry of each subunit but also the symmetry of the whole system have to be analyzed in order to determine the vanishing components of the

total second-order nonlinear response (hence the three columns labeled “ $C_i$ ” in Table II as far as centrosymmetry is concerned).

## 2. *Symmetry-driven discrimination of $\beta^{[0]}$ and $\beta^{[1]}$ response functions*

From Table I, we easily identify the composite diagrams which leave the nature of the molecular hyperpolarizability unchanged: types 0, 2, 4, 6 and 8 are characterized by  $\beta^{[1]}$  and  $\beta^{[0]}$  functions of the same kind. In this case, we recover the same situation as described earlier at the electric dipole level and applied to molecule-nanoparticle systems:<sup>12</sup> interaction with the partner modifies the molecular hyperpolarizability in amplitude and in phase but the molecular properties described by  $\beta^{[0]}$  are transferred to  $\beta^{[1]}$  for the bipartite system. In contrast, diagrams of types 1, 3, 5 and 7 involve hyperpolarizabilities of different natures, modified by the transfer from the isolated molecule to the bipartite system. For instance, in the type-5a diagram of Fig. 2, the molecule creates a dipole oscillating at the SFG frequency through an (eee) process (via  $\beta^{[0],eee}$ ) which couples to the partner through an (ee) coupling (via  $\mathbf{W}^{ee}$ ) and leads to the magnetic emission of SFG radiation by the partner through an (me) linear process (via  $\alpha^{me}$ ). Hence, this results in an (mee) hyperpolarizability for the bipartite system. Such a change in natures between  $\beta^{[1]}$  and  $\beta^{[0]}$  may have interesting consequences. For all the  $\beta^{[1]}$  tensors allowed under  $C_i$  symmetry in Table II, their response remains allowed even after isotropic averaging in a bulk. For types 1 and 5 in particular, the  $\beta^{[1]}$  molecular response, non-vanishing under isotropic averaging, arises from the  $\beta^{[0],eee}$  response of the molecule which conversely vanishes under the same isotropic averaging when considered alone. A change in symmetry due to interaction with the partner triggers in this case the generation of a bulk signal, transforming a material where bulk SFG is initially forbidden to one where bulk SFG is allowed by incorporating an appropriate partner in the system. In addition, as  $\beta^{[1]}$  and  $\beta^{[0]}$  do not obey the same selection rules, it becomes conceivable to experimentally tune the polarizations of light and the angles of incidence in order to favor one of them [as driven by Eqs. (34–38)] and quantify in this way the influence of the molecule-partner coupling.

### 3. *Spatial and spectral modulations of $\beta^{[1]}$*

Beyond the symmetry-driven selection rules associated to the respective response functions of the molecule, its partner and the composite system they form, the properties of the coupling matrix  $\mathbf{W}$  is obviously expected to play a pivotal role in the nonlinear response of the bipartite coupled system. Since the coupling constants  $\mathbf{W}$  strongly depend on the distance  $|\mathbf{R}|$  between the molecule and its partner, the resulting  $\beta^{[1]}$  function explicitly encompasses a spatial dependence. From Eqs. (10), (16) and (28) in Section III A, we see that  $\mathbf{W}(\mathbf{R})$  sums up contributions expressed as the zeroth, first and second powers of  $\omega|\mathbf{R}|/c$ , thus pertaining to the short, intermediate and long distances, respectively, and defining three “wave zones”. As known from classical dipolar emission and dipole-dipole coupling,<sup>16,58</sup> the short distance terms describe the static case and the long distance ones refer to radiation. The short distance approximation, typically for  $\omega|\mathbf{R}|/c \ll 1$ , applies in the visible and IR ranges to molecules in interactions with other molecules, nanoparticles of moderate size or a substrate. In that case, the leading terms behave like  $1/|\mathbf{R}|^3$  for  $\mathbf{W}^{ee}$  and  $\mathbf{W}^{mm}$ , and  $1/|\mathbf{R}|^4$  for  $\mathbf{W}^{Qe}$  and  $\mathbf{W}^{eQ}$ , while  $\mathbf{W}^{em}$  and  $\mathbf{W}^{me}$  are negligible as compared to (ee) and (mm). In other words,  $\mathbf{W}^{mm}$  must be included in our analysis as it is the sole contribution of magnetic interactions at short distances. As a consequence, only magnetic types 5a, 7b and 8 survive at short distances.

At first glance, the regime  $\omega|\mathbf{R}|/c \ll 1$  seems the most appropriate to describe local energy exchange between the partners. The decrease of  $\mathbf{W}$  amplitudes with  $|\mathbf{R}|$  makes the long distance approximation ( $\omega|\mathbf{R}|/c \gg 1$ ) less appealing for practical applications, unless it is compensated by high values of  $\alpha$ . We mainly count two interesting situations, therefore related to the behavior of  $\alpha$ . On the one hand, the linear polarizability of the partner may exhibit spectral resonances over the ranges of the input/output frequencies  $\omega_1$ ,  $\omega_2$  or  $\omega_3$ . In this way, coupling a molecule to a partner enables to enhance an intrinsically weak molecular response (which is in principle the case for all  $\beta^{[0]}$  except  $\beta^{[0],eee}$ ) through a high polarizability of the partner. For instance, it is not rare to play with specific (ee) resonances in the visible range like surface plasmon resonances,<sup>9,12</sup> gap-mode, SHINE-SFG,<sup>84</sup> and excitons.<sup>10</sup> In addition, the resonance frequencies associated with the electric, magnetic and quadrupolar polarizabilities may differ,<sup>70,85</sup> enabling a spectral separation between their respective contributions to  $\beta^{[1]}$ . On the other hand, the existence of a significant and possibly

resonant  $\alpha$  contribution may be strongly correlated to the distance regime of the associated coupling constants  $\mathbf{W}$ . This is the case for quadrupolar contributions, which are unavoidable as soon as the partner size approaches the wavelength of light. The need to consider the  $\alpha^{\text{QQ}}$  response of the partner concomitantly arises with a change in the distance regime from short to intermediate values of  $|\mathbf{R}| \sim \lambda$ , implying a longer-range  $\mathbf{W}^{\text{eQ/Qe}} \sim 1/|\mathbf{R}|^3$  (compared with the  $1/|\mathbf{R}|^4$  behavior of the static term). Here, the consideration of large-particle  $\alpha^{\text{QQ}}$  functions structurally goes hand in hand with the intermediate distance regime of the associated (eQ) and (Qe) coupling matrices. Strictly speaking, all terms in  $\mathbf{W}$  have to be taken into account for such intermediate distances  $|\mathbf{R}| \sim \lambda$  and it should be advisable to keep both the intermediate and radiation contributions as long as the short-distance approximation is not enforced. For example, it has been shown that the absorption of a dielectric nanoparticle is modified by phase-retarded coupling to a plasmonic partner through the intermediate distance terms of (ee), (mm) and (me/em)  $\mathbf{W}$  tensors.<sup>61</sup>

## V. PRACTICAL EXAMPLES

Among the various contributions to the SFG processes listed in Part III B, the user has to determine the leading and/or nonvanishing contributions in order to keep only the diagrams relevant for a given experiment. Of course, symmetry considerations are part of this selection process as discussed in Part IV, but the natures of both the molecule and the partner also play a major role. As detailed below, magnetic terms are relevant for chiral entities (either molecule or partner), in particular when their optical activities flows from their  $\alpha^{\text{em/me}}$  polarizabilities<sup>76</sup> through the so-called one-electron<sup>37</sup> or “ $\mu$ -m”<sup>38</sup> schemes. Quadrupolar contributions may meanwhile become important when the objects (i) are big enough to break the quasistatic approximation in the system (i.e. retardation and propagation of the electric fields have to be taken into account),<sup>74</sup> (ii) are too symmetric to generate only a dipolar response,<sup>19</sup> (iii) experience high electric field gradients at the boundary of a metallic or highly refractive medium,<sup>86</sup> or (iv) have their relative distance<sup>86</sup> much smaller than their sizes.<sup>87,88</sup> Both magnetic and quadrupolar polarizabilities also appear important to describe big spherical particles.<sup>50,61</sup> We now focus on some examples of systems for which the quadrupolar and magnetic bipartite diagrams become relevant.

## A. Quadrupolar contributions

As for the quadrupolar interactions, their contributions to the SFG response are expected to significantly grow when the partner size  $D_{\text{part}}$  increases, as compared to the wavelength of light  $\lambda$ , because of the growing importance of retardation effects. Still, even for objects with sizes  $D \ll \lambda$ , the dipole approximation (with respect to the electric multipole expansion) is known to fail to account for matter-matter interactions when the spatial gap  $\delta$  between the interacting objects is smaller than their sizes.<sup>87,89,90</sup> We may simply illustrate this by comparing the plasmonic properties of a molecule-nanosphere system, for which the inter-object gap is of the order of the molecular size, to those of a nanoparticle dimer in which the gap may be reduced far below the particle size. The first system is straightforwardly modeled in the dipolar approximation as long as  $D_{\text{part}} \ll \lambda$ ,<sup>14</sup> whereas it is well-known that the second system requires a multipolar description of the plasmonic interaction.<sup>88</sup> For other kinds of interactions, in the case of nanoscale fluorophores like semiconductor quantum dots<sup>87</sup> (4-10 nm in diameter) and carbon nanotubes<sup>89</sup> (0.6 nm  $\times$  3 nm), the resonant energy transfers occurring within pairs cannot be theoretically modeled by a strictly dipole-dipole coupling  $\mathbf{W}^{\text{ee}}$ . In this context, some theoretical works start examining the limits of Förster's dipole-dipole theory. For carbon nanotubes (which could play the role of the molecular species as well as the nanoscale partner in a molecule-partner system), X. Zhang *et al.* have shown that higher multipole interactions are determining,<sup>89</sup> favoring resonant energy transfers between dark states (i.e. dipole-forbidden) instead of bright states (i.e. dipole-allowed). We understand that the involvement and the nature of quadrupolar contributions in a bipartite system depend not only on the values of  $D_{\text{mol}}/\lambda$  and  $D_{\text{part}}/\lambda$ , but also on the spatial gap  $\delta$ , through the ratio  $\delta/\min(D_{\text{mol}}, D_{\text{part}})$ .

### 1. Energy transfer between small partners with small gap (type 2)

Here we consider systems for which the relative sizes of the two objects verify  $D_1, D_2 \ll \lambda$ , while  $\delta < \min(D_1, D_2)$ , as in the above-mentioned dimer of carbon nanotubes. We can easily draw the parallel between dark state-mediated resonant energy transfers and diagrams of type 2 (cf. Table II), which support the possibility of an enhanced (eee) contribution to the SFG response arising from an (eQ) coupling. In the same way as resonant energy transfers

between closely spaced nanoscale objects may be dominated by quadrupolar interactions, the hyperpolarizability  $\beta^{\text{eee}}$  of a big enough molecule coupled with a partner through a small gap could be mainly driven by  $\beta^{[0],\text{eee}}\mathbf{W}^{\text{eQ}}\boldsymbol{\alpha}^{\text{Qe}}$  (type 2) instead of  $\beta^{[0],\text{eee}}\mathbf{W}^{\text{ee}}\boldsymbol{\alpha}^{\text{ee}}$  (type 0), whatever the molecule initially described by  $\beta^{[0],\text{eee}}$ . Here, the role of  $\boldsymbol{\alpha}^{\text{Qe}}$  makes sense: on the one hand, the light-matter interaction between the incoming photon and the partner is governed by the length scale between the partner size  $D_{\text{part}}$  and the excitation wavelength  $\lambda$ , which justifies that the right index of  $\boldsymbol{\alpha}$  (i.e. its input) is electric dipolar; on the other hand, the matter-matter interaction between the molecule and its partner is driven by the length scale between their gap  $\delta$  and their smallest size, i.e.  $\min(D_{\text{mol}}, D_{\text{part}})$ , which justifies that the left index of  $\boldsymbol{\alpha}$  (i.e. its output) is quadrupolar within our hypotheses. Here we understand that the typical lengths and distances at play within the bipartite system define the wave zone and the nature of the coupling that must be considered as well as how to model the partner. In addition, symmetries also enter the game when nanoscale partners such as metal nanoparticles or semiconductor nanocrystals are involved. For such objects, synthesized through a bottom-up mechanism, a small size goes along with a lot of surface defects acting as sources of symmetry breaking and quantifying the departure from the perfect spherical symmetry:<sup>23</sup> even for such “symmetric” objects, nonvanishing  $\boldsymbol{\alpha}^{\text{Qe/eQ}}$  may be considered. Conversely, a growth in size often translates into an increasing degree of centrosymmetry as the surface defects lose their significance with the decrease of the surface-to-volume ratio. As a result, when the partner size grows,  $\boldsymbol{\alpha}^{\text{Qe/eQ}}$  tend to vanish and the surface-specific type-2 diagrams become negligible. However, this is counterbalanced by the rising of retardation effects and, schematically, type-2 SFG diagrams can be discarded to the benefit of type-1b diagrams, driven by  $\boldsymbol{\alpha}^{\text{QQ}} \neq \mathbf{0}$ .

## 2. *Quadrupolar SFG from large centrosymmetric partners (type 1b)*

It is useful to remind that the quadrupolar contribution is expected to be superseded itself by higher order multipole terms as the particle size increases. In order to design a  $\mathbf{W}^{\text{eQ}}$ -coupled bipartite system, the size of the partner must be carefully chosen so as to minimize both the dipolar and the octupolar contributions. In the case of colloidal silver nanoparticles, this quadrupolar regime is achieved for a diameter sizing around 160 nm with a quadrupolar resonance at  $\sim 450$  nm in wavelength, as deduced from UV-visible absorption

spectroscopy<sup>70</sup> (which is driven by, and hence gives access to,  $\alpha^{\text{QQ}}$ ). However, for the majority of the systems, we may expect the quadrupolar resonances to be accompanied by magnetic ones,<sup>85</sup> whatever the size. The discrimination between the  $\mathbf{W}^{\text{eQ}}$  and  $\mathbf{W}^{\text{em}}$  coupling regimes is then possible according to the frequency range over which we probe the system. In the case of silicon nanocubes, P. D. Terekhov *et al.*<sup>85</sup> theoretically showed that the optical scattering spectrum of parallelepipeds of 250 nm  $\times$  250 nm  $\times$  275 nm is dominated by (i) a quadrupolar resonance over the wavelength range 700-760 nm and (ii) two magnetic resonances below 700 nm. From such UV-visible spectra, it is then possible to extract the  $\alpha^{\text{QQ}}$  and  $\alpha^{\text{mm}}$  response functions associated to each set of resonances (note that Fresnel factors may have to be considered to properly relate the far-field resonances to response functions  $\alpha$ ), and to plug them into type-1b and type-5b diagrams in order to compute their respective contributions to the SFG response. In the context of IR-visible SFG spectroscopy, the resonant terms of the hyperpolarizability  $\beta^{[1]}$  of a molecule coupled with such a nanocube would typically read:

$$\begin{cases} \beta_{i\xi jk}^{[1],\text{eQe}}(\omega_1, \omega_2) = -\beta_{ihk}^{[0],\text{eee}}(\omega_1, \omega_2) W_{h\xi l}^{\text{eQ}}(\omega_1) \alpha_{\xi l \xi j}^{\text{QQ}}(\omega_1) & \text{if } \lambda_1 > 700 \text{ nm} \\ \beta_{ijk}^{[1],\text{eme}}(\omega_1, \omega_2) = -\beta_{ihk}^{[0],\text{eee}}(\omega_1, \omega_2) W_{hl}^{\text{em}}(\omega_1) \alpha_{lj}^{\text{mm}}(\omega_1) & \text{if } \lambda_1 < 700 \text{ nm} \end{cases}, \quad (39)$$

where  $\omega_1 = 2\pi c/\lambda_1$  scans the visible-near IR quadrupolar and magnetic resonances of the nanocube and  $\omega_2$  probes the IR vibrational response of the molecule [summation is implicit for all pairs of identical indices in Eq. (39)].

Interestingly, the electric dipole-quadrupole  $\mathbf{W}$  interactions become huge for metal nanoparticles arranged in 2D-array geometry.<sup>50,72</sup> Henceforth, even if type-1b diagrams do not lead to a surface-specific response (since bulk-allowed), the associated SFG contributions can be important for the study of nanostructured plasmonic substrates designed for surface-enhanced vibrational spectroscopy. As theoretically modeled by A. B. Evlyukhin *et al.*,<sup>50</sup> 600 nm-periodic hexagonal 2D arrays of 120 nm-sized gold nanoparticles exhibit a strong and sharp quadrupolar resonance at 770 nm and a broad quadrupolar band between 500 and 650 nm. Such a nanostructured surface would then constitute an appropriate substrate on which to graft molecular species for studying their  $\alpha^{\text{QQ}}$ -enhanced SFG response over the 500-800 nm wavelength range. By the same token, S. P. Hastings *et al.* have experimentally and theoretically demonstrated that immobilized spiky gold nanoshells

( $\sim 200$  nm in diameter) feature quadrupolar resonances which significantly enhance Raman scattering<sup>91</sup> (which is also a nonlinear optical process used for vibrational spectroscopy). While such plasmonic modes are nonradiating in the far-field wave zone, their contribution to the local field enhancement of molecules grafted on the spiky nanoshells (e.g. mercapto-benzoic acid<sup>91</sup>) is predominant and gives rise to the so-called Quadrupole-Enhanced Raman Scattering (QERS) process. SFG spectroscopy could similarly benefit from such quadrupolar near-field resonances through type-1b (and type-1a, for non-centrosymmetric partners) hyperpolarizabilities.

Furthermore, given that type-1 processes are bulk-allowed, coupling molecular analytes (e.g. solute molecules) with the aforementioned partners (e.g. silver nanoparticles, semiconductor quantum dots, carbon nanotubes, silicon nanocubes, spiky gold nanoshells) would also lead to resonantly enhanced (eQe/eeQ/Qee) SFG responses in colloidal suspensions, provided that the visible-near IR ( $\omega_1$ ) and/or the SFG ( $\omega_3$ ) frequencies coincide with the partner resonance modes. Depending on its degree of symmetry, we may for example reasonably expect a quadrupolar SFG emission mediated by the partner through  $\beta^{[1],Qee} = (\alpha^{Qe} \mathbf{W}^{ee} + \alpha^{QQ} \mathbf{W}^{Qe}) \beta^{[0],eee}$ , even though the quadrupolar resonances of  $\alpha^{Qe}$  (that is bulk-forbidden) and  $\alpha^{QQ}$  are not the dominant linear processes in the far-field when the partner is alone.

### 3. *SFG from molecular quadrupoles (type 4)*

A special attention must also be paid to diagrams of type 4, which are characterized by bulk-allowed (eQe/eeQ/Qee)  $\beta^{[1]}$  functions [like type 1, but with (ee) coupling and (ee) partner polarizability]. As soon as the bipartite systems follow an isotropic volume distribution, type-4 diagrams are the sole non-vanishing contributions involving the linear electric dipole response of the partner and thus arise as the leading ones (notwithstanding their magnetic counterparts of type 8). However, processes of type 4 may require molecular species which naturally feature quadrupolar behaviors through  $\beta^{[0]}$ . Three categories of molecular systems hence come to mind. (i) First, this occurs when the molecular structure exhibits a significant degree of symmetry, like nonpolar organic molecules or quadrupolar chromophores. For instance, in the vicinity of liquid/air interfaces, the SFG response of benzene has been ascribed to its quadrupole transition,<sup>33</sup> through a significant  $\beta^{[0],Qee}$  contribution.<sup>92</sup> Quite

recently, some benzene derivatives like ethylbenzene, toluene, benzaldehyde and aniline have also revealed such properties,<sup>79</sup> even though their respective substituents theoretically break the background centrosymmetry of benzene. In contrast, the interest of quadrupolar chromophores (e.g. D- $\pi$ -A- $\pi$ -D structures) for (eQe/eeQ/Qee) SFG is more ambiguous as they exhibit charge-transfer states with high dipole moments,<sup>93–96</sup> which somehow compensate the vanishing of their ground state dipole moments and may dominate any quadrupolar response. The dipolar versus quadrupolar origin of their second-order nonlinear properties has not been addressed in the literature and the potential of small quadrupolar chromophores like squaraine derivatives<sup>95,97</sup> as quadrupolar SFG probes remains an open question. (ii) Second, the antiparallel dimerization of identical molecules can introduce the inversion symmetry required to cancel their dipolar response. This has been observed by vibrational SFG spectroscopy for H-bond-stabilized acetic acid dimers,<sup>19</sup> whose IR resonance at 1712 cm<sup>-1</sup> has been assigned to the quadrupolar response of the C=O vibrations while the SFG amplitude appeared proportional to the volume concentration of dimers, confirming its bulk origin. In the same vein, polarization-resolved hyper-Rayleigh scattering (i.e. scattering SHG<sup>98</sup>) experiments have shown that mixed suspensions of cationic amphiphilic molecules featuring a strong  $\beta^{[0],eee}$  lose their electric dipole response after the increasing addition of an anionic surfactant (with zero  $\beta^{[0],eee}$ ) due to the appearance of centrosymmetric micelles characterized by a dominant quadrupolar  $\beta$  response.<sup>99</sup> (iii) Third and last, we can expect the intrinsic molecular response to be mainly quadrupole-driven when the electronic structure of the molecule is initially rich in dark states (i.e. dipole-forbidden excited states), as is the case for carbon nanotubes.<sup>89</sup>

## B. Magnetic contributions

For a system encompassing neither an external magnetic field nor a permanent magnetization,<sup>100</sup> there are essentially two kinds of magnetic contributions to the bipartite diagrams, differing by the origin of the magnetic response functions as defined in Parts II and III. In the first family, the magnetic contributions stem from the solid state (i.e. bulk) properties of the object. They are rather common for condensed matter objects like a solid substrate or a nanoparticle and follow from achiral components of the bulk-allowed response functions: polarizability  $\alpha^{mm}$ , hyperpolarizabilities  $\beta^{mee}$ ,  $\beta^{eme}$  and  $\beta^{eem}$ . The simplest example is given

by the Mie theory for spheres, for which the magnetic dipolar term is driven by coefficient  $b_1$ ,<sup>77</sup> allowing nanoparticles to participate to type-5b diagrams through  $\alpha^{\text{mm}}$ . For this kind of solid state processes, magnetic terms compete with the quadrupolar ones provided that electric field gradients reach high values, as is especially the case at the boundary of a metal. In addition, they suffer from their symmetry rules: for instance, the magnetic terms do not contribute to the SHG signals produced by nanospheres<sup>22</sup> or at the surface of a metal.<sup>17</sup> We may also mention that noble metal nanoparticles have been shown to exhibit magnetic properties,<sup>101,102</sup> but we have found no report of an influence on their optical properties in the absence of an external magnetic field.

The second family encompasses all magnetic contributions related to chirality or, beyond the sole molecular description, to optical activity. Diagrams involving chiral molecules, but also some objects like chiral nanostructures which contribute to the first family too, pertain to this second family. Chiral nanostructures, as well as chiral molecules, have nonvanishing  $\alpha^{\text{em/me}}$  response functions,<sup>45–48</sup> specific to chirality.<sup>44,103</sup> These rank-2 tensors contain the so-called “one-electron” chiral contribution to linear optics (in our multipartite system perspective, we choose to call it the single-object chiral response) and act as sources of optical rotation<sup>76,104,105</sup> and circular dichroism.<sup>106–108</sup> As a consequence, they may be experimentally determined or reconstructed from such elementary measurements. Conversely, the second-order response functions  $\beta$  of the (eee), (eem), (eme) and (mee) kinds encompass both chiral and achiral components,<sup>57</sup> so none of them is intrinsically specific of a chiral system. It has also been shown that the chirality of an experiment could arise by probing an achiral molecule under a chiral optical setup<sup>109</sup> or in a chiral supramolecular assembly.<sup>110</sup> Concentrating on the magnetic contributions to chirality (quadrupolar contributions may be neglected as far as chirality is concerned<sup>37,111</sup>), we understand that the situation differs between linear and second-order nonlinear optics. As for the former, they are essential to the description of optical activity whereas, for the latter, there is no general agreement on the need to include magnetic contributions in the analysis of chiral SHG or SFG response. As stated in Ref 112: “Clearly, there are still some lingering questions regarding the general conditions under which contributions beyond the electric dipole approximation are experimentally significant.”

In the literature, part of the publications show that magnetic contributions play a role in chiral molecular nonlinear response,<sup>51,103,113,114</sup> and that chiral magnetic components of

the second-order susceptibility may have the same order of magnitude as the chiral electric components,<sup>78,115</sup> while other papers succeed in interpreting experimental data using electric dipolar contributions only.<sup>66,116</sup> It is not central to the present paper to analyze the reasons for these discrepancies,<sup>112</sup> for which we simply provide a non-exhaustive list. These can indeed relate to: (i) the origin of chirality (there are essentially two kinds of molecular chirality as described in the SHG and SFG literature: the one-electron helical model<sup>117</sup> and the coupled oscillator model;<sup>118</sup> and it has been shown that second-order nonlinear optical response of the former involves magnetic components whereas they are not necessary for the latter<sup>37</sup>); (ii) the nature of the investigated system (for highly ordered or isotropic monolayers, thin and thick films, and chiral liquids, the balance between electric and magnetic contributions dramatically changes depending on the surface vs. bulk balance, and ordered vs. disordered molecular assembly; in chiral liquids for example, the magnetic contributions are estimated to vanish<sup>65</sup>); (iii) the experimental method, amongst SHG, homodyne or heterodyne SFG (e.g. chiral liquids produce SFG radiation but no SHG,<sup>119</sup> while heterodyne SFG helps separating surface from bulk chiral contributions);<sup>66</sup> (iv) the experimental observables (discrimination between enantiomers by SFG chiral<sup>120–122</sup> or differential<sup>123,124</sup> polarization schemes; optical rotatory dispersion in SHG,<sup>125</sup> linear and circular dichroisms in SHG<sup>126,127</sup> and SFG;<sup>128</sup> determination of a full set of electric and magnetic tensor components by continuous polarization tuning<sup>103</sup>); (v) the resonance phenomena (when vibrational or electronic resonances are involved, in the specific cases of IR activity, Franck-Condon vibronic coupling or breaking of the Born-Oppenheimer approximation, their selection rules and dispersion relation modulate the response; for example, vibrational SFG in chiral liquids requires an electronic resonance to enhance the antisymmetric part of the Raman tensor<sup>67,129</sup>); (vi) the interactions involved in the nonlinear process. In all situations for which the experimental conditions are not designed to separate electric from magnetic contributions, it is conceivable that some experimental signals attributed only to (eee) terms encompass in fact also inseparable magnetic contributions, in particular from the bulk.

### ***1. Review of the first-order chiral response***

As mentioned in point (i), the nature of chirality controls the properties of the chiral response. For single objects, the one-electron activity is enough.<sup>35,76,104,130,131</sup> However, op-

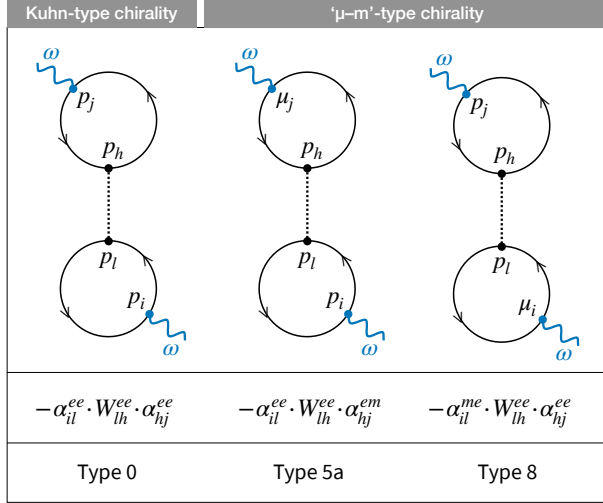


FIG. 3. Representative bipartite diagrams for linear response functions  $\alpha^{[1]}(\omega)$ . In this case, the asymmetry between molecule and partner is lost, as they are both the locations of  $\alpha$ -driven linear processes.

tical activity has been known for long to also stem from an assembly of chiral or achiral objects. Apart from the supramolecular assemblies of oriented achiral entities,<sup>110</sup> there is a huge literature on the optical activity of coupled noncoplanar dipoles<sup>132</sup> and, more generally, of polymers and peptides described as aggregates of identical monomers in interaction, either randomly or partially oriented.<sup>108</sup> For such systems, there are three sources of optical activity:<sup>38,133</sup> the single-object response (driven by  $\alpha^{em}$  and  $\alpha^{me}$ ), the coupled electric dipolar response (chirality of the Kuhn type<sup>132,134</sup>) and the coupled electric-magnetic dipolar response (chirality of the “ $\mu$ -m” type<sup>38</sup>). Several equivalent methods have been established in order to account for such effects,<sup>108</sup> either by quantum mechanical<sup>40,133</sup> or classical approaches.<sup>13</sup> They consider optical activity created and modified by dipole-dipole coupling (i.e. involving  $\mathbf{W}^{ee}$ ) between monomers. In other words, they take into account the influence of the diagrams of types 5a and 8 (more precisely, their counterparts in linear optics, which are in fact symmetric between molecule and partner) and also, more unexpectedly, of the diagrams of type 0. Figure 3 illustrates these three cases, giving rise to bipartite  $\alpha^{[1]}$  response functions.

In order to briefly review the origins of such processes, we consider a bipartite system wherein partner and molecule are identical. Contrary to the single-object chirality, the chiral response of noncoplanar coupled dipoles remains fully described by electric dipolar contributions as it only involves two electric dipoles oscillating at the partner and the molecule (a

classical interpretation shows the equivalence with a hybrid electric-magnetic mechanism<sup>38</sup>). In the diagrammatic perspective, this mechanism is simply represented by a type-0 diagram of the first order response function  $\boldsymbol{\alpha}^{[1],ee}$  (Fig. 3). In the literature,  $\mathbf{W}^{ee}$  is usually considered at the static level,<sup>134</sup> meaning that no  $\omega|\mathbf{R}|/c$  retardation term is considered in Eq. (10) as for the energy transfer. However, retardation in the propagation of the light beam traveling from partner to molecule, neglected up to now, is taken into account through a factor  $e^{i\mathbf{k}\cdot(\mathbf{r}_2-\mathbf{r}_1)} = e^{-i\mathbf{k}\cdot\mathbf{R}}$ , where  $\mathbf{k} = \omega/c\hat{\mathbf{k}}$  is the wavevector of light. A plane wave description is again assumed. At first order,  $e^{-i\mathbf{k}\cdot\mathbf{R}} \approx 1 - i\mathbf{k}\cdot\mathbf{R}$  and the coupling constant in Eq. (9) is modified into:

$$(C_{ab,mn}^{ee})_{\text{retarded}} \approx \sum_{h,l} p_{ab}^l W_{lh}^{ee} (1 - i\mathbf{k}\cdot\mathbf{R}) p_{mn}^h = C_{ab,mn}^{ee} + (C_{ab,mn}^{ee})_{\text{chiral}}, \quad (40)$$

where  $p_{ab}^l$  and  $p_{mn}^h$  refer to the molecule and the partner, respectively. The first term is responsible for the  $\boldsymbol{\alpha}^{[1],ee}$  response due to the achiral electric dipole-dipole coupling. Retaining only the second term, responsible for the chiral response, we plug it into a bipartite diagram (Fig. 3, type 0) to get:

$$[\alpha_{ij}^{[1],ee}(\omega)]_{\text{chiral}} = \frac{\omega}{c}(\hat{\mathbf{k}}\cdot\mathbf{R}) \sum_{l,h} \alpha_{il}^{ee}(\omega) W_{lh}^{ee}(\omega) \alpha_{hj}^{ee}(\omega). \quad (41)$$

Here,  $\boldsymbol{\alpha}$  is the polarizability of each object inside the system, which also integrates the effects of the  $C_{ab,mn}^{ee}$  couplings, leading for example to excitonic splitting.<sup>135,136</sup> In an isotropic material, the rigid bipartite system may take any orientation with respect to the laboratory axes. Using the properties of rotational averaging<sup>105</sup>  $\langle \mathbf{T} \rangle_{ijk} = -1/6 \left( \sum_{i,j,k} T_{\alpha\beta\gamma} \epsilon_{\alpha\beta\gamma} \right) \epsilon_{ijk}$  over the third rank tensor  $T_{ijk} = \sum_{l,h} \alpha_{il}^{ee} W_{lh}^{ee}(\omega) \alpha_{hj}^{ee} R_k$ , we see that only the terms with  $i, j, k$  all different survive. We note that this is the essence of a chiral response, which requires to involve the three directions of space and changes sign with the handedness. If we fix  $\hat{\mathbf{j}}$  as the direction of the electric field  $\mathbf{E} = |\mathbf{E}|\hat{\mathbf{j}}$ , the average electric dipole created by  $\langle \boldsymbol{\alpha}_{\text{chiral}}^{[1],ee} \rangle_{ij}$  is oriented along  $\hat{\mathbf{i}}$ , i.e. along the magnetic field  $\mathbf{B} = -|\mathbf{E}|/c\hat{\mathbf{i}}$ . We have:

$$\langle \mathbf{p}_{\text{chiral}} \rangle = \langle \boldsymbol{\alpha}_{\text{chiral}}^{[1],ee} \rangle_{ij} |\mathbf{E}| \hat{\mathbf{i}} = \frac{\omega}{6}(\hat{\mathbf{k}}\cdot\mathbf{R}) \sum_{l,h} \alpha_{il}^{ee} W_{lh}^{ee} \alpha_{hj}^{ee} \mathbf{B}. \quad (42)$$

Using the Maxwell-Faraday equation  $\omega\mathbf{B} = \nabla \times \mathbf{E}$ , we recover  $\langle \mathbf{p}_{\text{chiral}} \rangle = g\nabla \times \mathbf{E}$ , where

$g$  is given by the Kirkwood equation<sup>105,134,137</sup> and quantifies the chiral response (e.g. optical rotation).<sup>138,139</sup> We note that, in the literature, Eq. (40) is equivalently transformed into the projection of the quantity  $\mathbf{R} \cdot (\mathbf{p}_{\text{mol}} \times \mathbf{p}_{\text{partner}})$  onto states  $(a, b, m, n)$ , which becomes the source of chirality.<sup>13,40,108,140</sup> For practical systems involving polymers, the scheme is extended to an arbitrary number of monomers by summing up over monomers and using the self-consistent achiral polarizability as  $\alpha$ , this quantity being easily accessed by linear (e.g. absorption) spectroscopy.

In the “ $\mu$ - $m$ ” scheme (that we could call here “ $p$ - $\mu$ ” scheme, as we depict the electric and magnetic dipoles by  $\mathbf{p}$  and  $\boldsymbol{\mu}$ , respectively, whereas  $\boldsymbol{\mu}$  and  $\mathbf{m}$  are often used instead in the original literature on the subject), chirality stems from a molecule-partner interaction wherein the light-induced dipolar transition moments are, on the one hand, electric (resp. magnetic) at the molecule and, on the other hand, magnetic (resp. electric) at the partner.<sup>13,40,108</sup> In terms of our diagrammatic description of the first-order response, it involves diagrams of types 5a and 8 (Fig. 3), where the chiral response of the bipartite system is driven by:

$$-\alpha_{ij}^{[1],\text{em}}(\omega) = \alpha_{il}^{\text{ee}}(\omega)W_{lh}^{\text{ee}}(\omega)\alpha_{hj}^{\text{em}}(\omega), \quad (43)$$

and:

$$-\alpha_{ij}^{[1],\text{me}}(\omega) = \alpha_{il}^{\text{me}}(\omega)W_{lh}^{\text{ee}}(\omega)\alpha_{hj}^{\text{ee}}(\omega), \quad (44)$$

respectively. Diagrams of types 5b, 6 and 7 are not considered in the literature because, as it is sometimes stated:<sup>38</sup> “magnetic dipoles do not couple directly with electric dipoles.” This is true when only electric dipolar interaction ( $\mathbf{W}^{\text{ee}}$ ) between molecule and partner is considered. Attempts to extend this coupling to quadrupolar interaction have been made,<sup>38</sup> but not to  $\mathbf{W}^{\text{em}}$  and  $\mathbf{W}^{\text{me}}$ . The underlying hypothesis is that only the static terms for interaction are considered, leaving only (ee), (eQ), (Qe) and, with a lower magnitude, (mm)  $\mathbf{W}$  tensors. When these tensors are extended to include retardation of the dipole and quadrupole radiations [i.e.  $\omega|\mathbf{R}|/c$  contributions in Eq. (10), (28) and (31)], new types of processes become allowed. We indeed wonder why retardation should be taken into account [Eq. (40)] in the propagation of light beams to account for the response of coupled dipoles, but not in the interaction Hamiltonians. These new processes mediated by  $\mathbf{W}^{\text{em}}$  and  $\mathbf{W}^{\text{me}}$  mix the single-object achiral ( $\alpha^{\text{ee}}$ ) and chiral ( $\alpha^{\text{em/me}}$ ) responses to generate an electric dipolar response. This time, the “ $\mu$ - $m$ ” coupling is buried inside the system, still leading to

a chiral response.

## 2. *Second-order response*

By analogy with linear optics, the three sources of chirality listed in the previous Part build up the chiral response functions of nonlinear optics in multipartite systems. Chirality of the response is to be estimated on the basis of the complete  $\beta^{[1]}$  function but, as will be briefly detailed below, we have to distinguish three cases corresponding to the three schemes listed in Part VB 1: the chiral response may be located at the molecule (single-object scheme), at the partner (“ $\mu$ -m” scheme) or result from the chiral interaction between both (coupled oscillators). In the single-object scheme, the molecule is fully responsible for the chiral response and directly generates (eee), (eem), (eme) and (mee) responses at the  $\beta^{[0]}$  level.<sup>37,117</sup> It does not need coupling with a partner but, as in the electric dipole approximation, the response functions are modified by the presence of any kind of achiral partner in types 0, 5b, 7a and 8 diagrams. The coupled dipoles have been extensively used to describe the chiral SFG response of molecules like binaphthol in a phenomenological point of view: the bipartite system is considered as a whole and the chiral properties of  $\beta^{[1]}$  follow from the contraction with the Levi-Civita tensor  $\epsilon_{ijk}$  upon rotational averaging<sup>141</sup> and from the underlying  $\mathbf{R} \cdot (\mathbf{p} \times \mathbf{p})$  scheme.<sup>128,140</sup> Other descriptions follow from the mechanical oscillations of electrons with coupled moves.<sup>37,139</sup> To our knowledge, a description of the chiral SFG response of noncoplanar dipoles in terms of type-0 diagrams, i.e. in the same line as the Kirkwood equation, has never been considered. We note that such a “Kirkwood-like” description would make it easier to introduce the resonant processes required for the nonvanishing of the chiral response.<sup>37,65,142</sup> Finally, in the “ $\mu$ -m” schemes, the magnetic contribution required to induce a chiral response is set on the partner through  $\alpha^{\text{em}}$  and  $\alpha^{\text{me}}$ , and transferred to the molecule in type-5a, -6 and -7b diagrams. This time, only the partner needs to be chiral, which is of course the case as far as a chiral polymer is concerned, but may also apply to a chiral nanoparticle coupled to an achiral molecule. We note the particular case of type 7b, for which the chiral response may be considered on either the molecule or the partner.

For identical molecule and partner, type-5a diagrams transform an electric dipolar (eee)  $\beta^{[0]}$  response into a mixed electric-magnetic response by coupling to neighboring molecules

through their  $\alpha^{\text{me/em}}$ , while the same kind of response is conversely generated in type-8 diagrams from a mixed (eem), (eme), (mee)  $\beta^{[0]}$  molecular response through the usual (ee) polarizability. Both types rely on electric dipole-dipole coupling. This illustrates the difference between nonlinear (Fig. 2) and linear (Fig. 3) optics: for the former, the coupled tensors  $\beta^{[0]}$  and  $\alpha$  refer to different optical processes. In other words, the role of each object is well defined. For the latter, the  $\alpha$  response is common to molecule and partner, making it necessary to use a self-consistent method to establish the link between the polarizabilities of the monomers with and without coupling. When dealing with the second order response, it is implicitly assumed that all the couplings have already been included at first order, so that the  $\alpha$  response functions to be used in the implementation of the method (e.g. types 5a and 8) are those of the coupled system. As such, they directly flow from experimental data (e.g. absorption for  $\alpha^{\text{ee}}$ , optical rotation or circular dichroism for  $\alpha^{\text{me/em}}$ ).

In addition to types 5a and 8, the other types relate on electric-magnetic or magnetic-magnetic dipole-dipole coupling, usually discarded in the literature. These are interesting for two reasons. First, in types 5 and 7, the coupling transforms a mixed electric-magnetic  $\beta$  response into an (eee) response (and vice versa). For type 7a in particular, this is done by coupling to the dominant (ee) molecular polarizability (still in the case of identical molecule and partner). The consequence is that a part of the monomer (mee/eme/eem) response [resp. of the monomer (eee) response] is experimentally measured as an (eee) contribution [resp. a (mee/eme/eem) contribution] in the bipartite system. Depending on the order inside the sample, and on the presence of bulk contributions, the sum of all the contributions of types 0, 5, 6, 7 and 8 may tune the balance between (eee) and mixed (mee/eme/eem) terms. It appears interesting to investigate their influence on the debated relative magnitudes of electric and magnetic terms in the SHG and SFG responses. Second, for all types of diagrams, the coupling makes it possible to modify the  $(ijk)$  indexing of a second-order tensor component. Consequently, as there are chiral and achiral components for each kind of tensor, it is possible to create a chiral  $\beta^{[1]}$  response from an achiral  $\beta^{[0]}$  and vice versa. This is a purely nonlinear optical effect as the equivalent does not exist in linear optics.

## VI. CONCLUSION

Second-order nonlinear processes like SHG and SFG have always been exploited for their symmetry properties, in relation with the geometry of the probed material. This directly results from the fact that nonlinear optics is essentially described in the literature within the frame of the electric dipolar approximation. Still, the question of the physical origins of the SFG signals actually measured in an experiment (surface vs. bulk, chiral vs. achi-ral) also closely relates to the electric quadrupolar and magnetic dipolar responses of the probed materials. Such quadrupolar and magnetic contributions are partially considered in the literature to account for the first hyperpolarizabilities of simple molecular systems (i.e. single objects). Here, we provide a comprehensive study of the quadrupolar and magnetic contributions to SFG in the more complex case of bipartite composite systems, based on the diagrammatic theory of nonlinear optics that we have developed earlier. In accordance with the multipolar expansion of electromagnetic interactions, we generalize our formalism, previously applied at the electric dipole level ('e'), to the electric quadrupole ('Q') and magnetic dipole ('m') levels of theory. We then introduce new one- and two-loop diagrams dedicated to the computation of hybrid 'e-Q' and 'e-m' optical response functions, and thus generate a set of new nonlinear mechanisms sorted according to their specific symmetry rules and the systems they apply to. In particular, we examine the consequences of our formal results on molecule-nanoparticle and molecule-molecule binary systems. For the former, the quadrupolar contributions enable us to account for size effects and non-dipolar electronic enhancement: depending on the sizes of the molecule, the nanoscale partner and their gap, the quadrupolar response may become dominant and resonant with the input and output light beams. Quadrupole-enhanced SFG thus appears as an interesting development path for vibrational spectroscopy. As for bipartite systems made of two identical molecules, our diagrammatic treatment of magnetic contributions proves to account well for chiral SFG: considering a single molecule as a monomer, we especially describe how loop diagrams can be used to build up the chiral response of molecular aggregates and polymers, formalizing the connection between the three classical schemes of chirality (i.e. one-electron model, Kuhn-Kirkwood mechanism and hybrid electric-magnetic dipole coupling).

Hence, this article provides a unified formalism to treat the electric dipole-, electric quadrupole- and magnetic dipole-driven linear and nonlinear optical responses of composite

systems. We have particularly focused on relating our approach to the existing literature in order to place our work in the continuity of established formalisms. The tools that are elaborated here are designed for a straightforward implementation and are illustrated with various well-known and exploratory systems, which are as many development paths and new tracks for experimenters and theoreticians.

## Appendix A: Computation method for composite loop diagrams

As developed in Refs. 11 and 12, the computation of a loop diagram is based on twelve Feynman rules. We do not reproduce these rules here (we refer the reader to the original publications) but briefly list the steps of the computation. As it describes an optical response function, a diagram generally consists of (i) several loops, representing the entities (or subsystems) composing the system and connected by interaction bosons, and (ii) photons, representing the interactions of the system with the outside (i.e. the inputs and output of the response function). Computation first consists in identifying the order of the response function from the number  $N_p$  of photons involved. Each diagram involving  $N_p$  photons is associated to an  $(N_p - 1)^{\text{th}}$ -order function: whatever its number  $N_l$  of loops, a diagram represents a first-order  $\alpha$  function for  $N_p = 2$  and a second-order  $\beta$  function for  $N_p = 3$ . The diagram is also characterized by the number  $N_v$  of interaction processes, each one taking place at a vertex located on a loop: we count  $N_p$  light-matter interactions (between the photons and the subsystems) and  $(N_v - N_p)$  matter-matter interactions (between the subsystems), mediated by interaction bosons. We remind that two vertices linked by a boson only count for one interaction process. For each interaction indexed by  $i \in \llbracket 1, N_v \rrbracket$ , the associated coupling constant  $C_i$  derives from the corresponding interaction Hamiltonian: it is defined by Eq. (8) and (9) for a matter-matter interaction, and simply reads  $p_{nm}^j$ ,  $\mu_{nm}^j$  and  $q_{nm}^{\xi j}$  for dipolar, magnetic and quadrupolar light-matter interactions, respectively, projected over the polarization of light  $j$ . All  $C_i$  include a sum over the quantum states of the subsystem(s) involved in the interaction process (e.g.  $\{abmn\}$  in Eq. (9) for matter-matter interaction and  $\{mn\}$  for light-matter interaction).

For interested readers, we describe here the “machinery” leading to the response functions in their final form in imaginary frequencies. Other readers may skip this paragraph. For each of the  $N_l$  loops, we assign an implicit Matsubara frequency (e.g.,  $\omega_\nu$ ) to the propagator associated to the initial state of the subsystem. We then apply the energy conservation (in terms of imaginary frequencies) at each vertex by ensuring that the constitutive energy relationship (e.g.,  $\omega_3 = \omega_1 + i\omega_2$ ) applies at one and only one vertex. Each loop now appears as a set of interaction vertices (to which a coupling constant  $C_i$  is assigned), responsible for a change in quantum states as described by  $C_i$ , and linked by propagators describing the evolution of their corresponding quantum state. Each propagator is thus associated to

an imaginary-time Green's function  $\mathfrak{G}_{nn}(i\omega_\nu + i\omega_n)$  where  $n$  is the label of the quantum state and  $i\omega_n$  the imaginary frequency that has been assigned to it by the conservation of energy (it can be checked that  $\omega_n$  is necessarily a positive or negative photon frequency, or zero). The response function of the diagram is obtained by multiplying the coupling constants  $C_i$  and the imaginary-time Green's functions, and summing their product over all the implicit Matsubara frequencies and the quantum states. The sum must be weighted by  $(-1)^{N_p+1} \cdot b^{N_p-N_v-1} \cdot \hbar^{N_p-2N_v}$ , where  $1/b = k_B T$  is the thermal energy. The response function  $f$  thus gets the following generic form:

$$f(\omega_1, \dots, \omega_{N_p-1}) = \frac{(-1)^{N_p+1}}{b^{-N_p+N_v+1} \hbar^{-N_p+2N_v}} \sum_{\{\nu\}} \sum_{\{n\}} \prod_n \mathfrak{G}_{nn}(i\omega_\nu + i\omega_n) \prod_{i=1}^{N_v} C_i, \quad (\text{A1})$$

where the first sum is over the set of the  $N_l$  Matsubara frequencies and the second one over the set of all quantum states. For diagrams involving loops linked by two or more bosons (which does not apply in the present article), additional rules and approximations apply, detailed in the Supplementary Material of Ref. 12. The sum over Matsubara frequencies is solved by application of the residue theorem, along the lines recalled in Ref. 11.

For diagrams involving only one loop (i.e., only light-matter  $C_i$  constants), the residue theorem generates a sum of  $N_p$  terms. Each term relates to one of the propagators (reference state, e.g.  $m$ ) and is the product of the  $N_p$  coupling constants  $C_i$  weighted by the density matrix diagonal element of the reference state  $\hat{\rho}_{mm}$ , and  $(N_p - 1)$  energy denominators containing the energy difference between the reference state and all the other states in the loop. The total elementary response function is obtained by summing all the different diagrams corresponding to the  $(N_p - 1)!$  permutations of the photons. First-order response functions  $\alpha$  thus sum up two terms [Eq. (2)], and second-order  $\beta$  functions group  $3 \times 2 = 6$  terms [Eq. (3)]. For diagrams involving several loops, the sums over Matsubara frequencies are separable, one per loop: each sum transforms the product of light-matter  $C_i$  and  $\mathfrak{G}_{nn}(i\omega)$  associated to this loop into an elementary response function. The full diagram therefore involves a matrix product (or a tensor contraction) of elementary response functions and matter-matter coupling constants, as is seen in Eq. (34–38). The diagram can be directly read in this case by following the energy flow of each photon from right to left as illustrated in Fig. 2.

## Appendix B: Elementary response functions

From the diagram in Fig. 1i, we use the Feynman rules<sup>11</sup> to deduce the  $\{i, j\}$  term of the tensor  $\alpha^{\text{em}}$ :

$$\alpha_{ij}^{\text{em}}(i\omega) = \frac{(-1)^3}{\hbar^2 b} \sum_{n,m;\nu} p_{mn}^i \mu_{nm}^j \mathfrak{G}_{mm}(i\omega_\nu) \mathfrak{G}_{nn}(i\omega_\nu + i\omega), \quad (\text{B1})$$

where  $\mathfrak{G}_{mm}(i\omega_\nu)$  is the imaginary-time Green function of state  $|m\rangle$  and  $b = 1/k_B T$ . Applying the residue theorem to Eq. (B1) gives:

$$\alpha_{ij}^{\text{em}}(i\omega) = -\frac{1}{\hbar} \sum_{n,m} p_{mn}^i \mu_{nm}^j \frac{\rho(\omega_m) - \rho(\omega_n)}{\omega_m - \omega_n + i\omega} \quad (\text{B2})$$

where  $\rho(\omega)$  is the Fermi-Dirac distribution. Using the equivalence between  $\rho(\omega_m)$  and  $\hat{\rho}_{mm}$ ,<sup>11</sup> we have:

$$\alpha_{ij}^{\text{em}}(i\omega) = \frac{1}{\hbar} \sum_{n,m} \hat{\rho}_{mm} \left( \frac{p_{mn}^i \mu_{nm}^j}{\omega_{nm} - i\omega} + \frac{\mu_{mn}^j p_{nm}^i}{\omega_{nm} + i\omega} \right), \quad (\text{B3})$$

where  $\omega_{nm} = \omega_n - \omega_m$ . Identically, we have:

$$\alpha_{ij}^{\text{me}}(i\omega) = \frac{1}{\hbar} \sum_{n,m} \hat{\rho}_{mm} \left( \frac{\mu_{mn}^i p_{nm}^j}{\omega_{nm} - i\omega} + \frac{p_{mn}^j \mu_{nm}^i}{\omega_{nm} + i\omega} \right). \quad (\text{B4})$$

It can be checked that both quantities are related by  $\alpha_{ij}^{\text{me}}(i\omega) = \alpha_{ji}^{\text{em}}(-i\omega)$ . In addition, when they apply to a molecule, the wavefunctions of the states may be considered real, and the dipolar and magnetic transition moments become real and imaginary, respectively.<sup>36,107</sup> Using the fact that, for Hermitian operators, transposed matrix elements are conjugated, we get in this particular case  $\alpha_{ij}^{\text{me}}(i\omega) = -\alpha_{ji}^{\text{em}}(i\omega)$ , which may be generalized to chiral reciprocal entities.<sup>47</sup>

From the diagram drawn in Fig. 1c representing  $\alpha^{\text{eQ}}$ , we get in the same manner:

$$\alpha_{i\xi j}^{\text{eQ}}(i\omega) = \frac{(-1)^3}{2\hbar^2 b} \sum_{n,m;\nu} p_{mn}^i q_{nm}^{\xi j} \mathfrak{G}_{mm}(i\omega_\nu) \mathfrak{G}_{nn}(i\omega_\nu + i\omega). \quad (\text{B5})$$

The main difference with  $\alpha^{\text{em}}$  lies in the tensor rank, which is here increased to 3 because of the matrix nature of  $\mathbf{q} = (q^{\xi i})$ . Since the residue theorem only applies to the sum over  $\nu$  [i.e.  $\frac{1}{b} \sum_{\nu} \mathfrak{G}_{mm}(i\omega_\nu) \mathfrak{G}_{nn}(i\omega_\nu + i\omega)$ ], the computation of  $\alpha_{i\xi j}^{\text{eQ}}$  is formally the same as that of

$\alpha_{ij}^{\text{em}}$ , simply changing  $\mu^j$  into  $\frac{1}{2}q^{\xi j}$ :

$$\alpha_{i\xi j}^{\text{eQ}}(\omega) = \frac{1}{2\hbar} \sum_{n,m} \hat{\rho}_{mm} \left( \frac{p_{mn}^i q_{nm}^{\xi j}}{\omega_{nm} - \omega} + \frac{q_{mn}^{\xi j} p_{nm}^i}{\omega_{nm} + \omega} \right). \quad (\text{B6})$$

Identically, we have:

$$\alpha_{\xi ij}^{\text{Qe}}(\omega) = \frac{1}{2\hbar} \sum_{n,m} \hat{\rho}_{mm} \left( \frac{q_{mn}^{\xi i} p_{nm}^j}{\omega_{nm} - \omega} + \frac{p_{mn}^j q_{nm}^{\xi i}}{\omega_{nm} + \omega} \right). \quad (\text{B7})$$

Eqs. (B6) and (B7) coincide with the perturbative expressions obtained by A. Morita<sup>143</sup> [Eqs. (10) and (9) in this reference, respectively] and C. Neipert *et al.*<sup>144</sup> [Eqs. (2.13) and (2.14) in this reference, respectively]. It can also be checked that  $\alpha_{i\xi j}^{\text{eQ}}(\omega) = \alpha_{\xi ji}^{\text{Qe}}(-\omega)$ .

The previous examples illustrate the fact that elementary functions involving one magnetic dipole (resp. electric quadrupole) vertex may be easily deduced from the purely electric dipolar ones by replacing the corresponding electric transition dipole by its magnetic (resp. quadrupolar) analogue.<sup>145,146</sup> Consequently, the generic term of tensors  $\beta^{\text{eem}}$ ,  $\beta^{\text{eme}}$  and  $\beta^{\text{mee}}$  (resp.  $\beta^{\text{eeQ}}$ ,  $\beta^{\text{eQe}}$  and  $\beta^{\text{Qee}}$ ) are deduced from Eq. (3) by replacing  $p^k$ ,  $p^j$  and  $p^i$  transition moments by  $\mu^k$ ,  $\mu^j$  and  $\mu^i$  (resp.  $\frac{1}{2}q^{\xi k}$ ,  $\frac{1}{2}q^{\xi j}$  and  $\frac{1}{2}q^{\xi i}$ ), respectively. This is actually very general for magnetic and quadrupolar terms, and flows from the expressions of the corresponding terms in the light-matter interaction Hamiltonian.<sup>147</sup> As an example, the generic term for  $\beta^{\text{eem}}$  is given by:

$$\beta_{ijk}^{\text{eem}}(\omega_1, \omega_2) = \frac{1}{\hbar^2} \sum_{m,n,r} \hat{\rho}_{rr} \left[ \frac{p_{rn}^i p_{nm}^j \mu_{mr}^k}{(\omega_{nr} - \omega_3)(\omega_{mr} - \omega_2)} + \frac{p_{mn}^i p_{nr}^j \mu_{rm}^k}{(\omega_{rm} - \omega_2)(\omega_{rn} + \omega_1)} \right. \\ \left. + \frac{p_{mr}^i p_{rn}^j \mu_{nm}^k}{(\omega_{mr} + \omega_3)(\omega_{nr} + \omega_1)} + \frac{p_{rn}^i p_{mr}^j \mu_{nm}^k}{(\omega_{nr} - \omega_3)(\omega_{mr} - \omega_1)} \right. \\ \left. + \frac{p_{mn}^i p_{rm}^j \mu_{nr}^k}{(\omega_{rm} - \omega_1)(\omega_{rn} + \omega_2)} + \frac{p_{mr}^i p_{nm}^j \mu_{rn}^k}{(\omega_{mr} + \omega_3)(\omega_{nr} + \omega_2)} \right]. \quad (\text{B8})$$

The last three terms of the bracket are deduced from the application of Feynman rules to the diagram of Fig. 1k, while the first three ones flow from its brother diagram (1  $\leftrightarrow$  2) obtained by permutation of the two inputs ( $E_j$ ,  $\omega_1$ ,  $p^j$ ) and ( $B_k$ ,  $\omega_2$ ,  $\mu^k$ ). In the same manner, we

can straightforwardly write the quadrupolar contribution  $\beta^{\text{Qee}}$  for instance:

$$\beta_{\xi_{ijk}}^{\text{Qee}}(\omega_1, \omega_2) = \frac{1}{2\hbar^2} \sum_{m,n,r} \hat{\rho}_{rr} \left[ \frac{q_{rn}^{\xi i} p_{nm}^j p_{mr}^k}{(\omega_{nr} - \omega_3)(\omega_{mr} - \omega_2)} + \frac{q_{mn}^{\xi i} p_{nr}^j p_{rm}^k}{(\omega_{rm} - \omega_2)(\omega_{rn} + \omega_1)} \right. \\ \left. + \frac{q_{mr}^{\xi i} p_{rn}^j p_{nm}^k}{(\omega_{mr} + \omega_3)(\omega_{nr} + \omega_1)} + \frac{q_{rn}^{\xi i} p_{mr}^j p_{nm}^k}{(\omega_{nr} - \omega_3)(\omega_{mr} - \omega_1)} \right. \\ \left. + \frac{q_{mn}^{\xi i} p_{rm}^j p_{nr}^k}{(\omega_{rm} - \omega_1)(\omega_{rn} + \omega_2)} + \frac{q_{mr}^{\xi i} p_{nm}^j p_{rn}^k}{(\omega_{mr} + \omega_3)(\omega_{nr} + \omega_2)} \right]. \quad (\text{B9})$$

It is identical to the expansion made by A. Perry *et al.*<sup>148</sup>, for whom the hyperpolarizability tensor is named and indexed  $\chi_{ijkl}^{\text{Qs}}(\omega_{\text{vis}}, \omega_{\text{IR}})$  in the context of vis-IR SFG spectroscopy [see Eq. (40) of this reference].

## Appendix C: Fresnel factors for hybrid electric-magnetic response functions

We consider a three-layer model consisting of two infinite plane interfaces [in the  $(\hat{\mathbf{x}}, \hat{\mathbf{y}})$  plane] separating three media labelled [1], [2] and [3], each characterized by a complex refractive index (e.g.  $n^{[1]}$ ). Thickness of medium [2], where the nonlinear process takes place, is supposed negligible as compared to the wavelength of light. The input light beams ( $i = 1, 2$ ) are incident (wavevector  $\mathbf{k}_i = \omega_i/c \hat{\mathbf{k}}_i$ , angle of incidence  $\theta_i^{[1]}$ ) on the system from medium [1] and SFG is emitted at  $\omega_3$  towards the same medium in reflection. For a more complete description of the model and notations, please refer to Ref. 57 and 4. Fresnel factors for the incoming beams relate  $E^{[2]}(\omega_i)$  and  $B^{[2]}(\omega_i)$ , the field amplitudes inside layer [2], to the far electric field amplitude  $E^0(\omega_i)$  in medium [1]. We have  $E_\alpha^{[2]}(\omega_i) = F_\alpha(\omega_i) E^0(\omega_i) e_\alpha^{[1]}(\omega_i)$ , where  $\alpha$  stands for  $\{x, y, z\}$  and  $e_\alpha^{[1]}(\omega_i)$  is the projection of the unit polarization vector of light  $\hat{\mathbf{e}}^{[1]}(\omega_i)$ , i.e. a combination of its  $\hat{\mathbf{s}}_i$  and  $\hat{\mathbf{p}}_i$  unit vectors, onto coordinate  $\alpha$ . Values for  $F_\alpha(\omega_i)$  may be written in short notation  $F_x(\omega_i) = [1 - r_p^{13}(\omega_i)]$ ,  $F_y(\omega_i) = [1 + r_s^{13}(\omega_i)]$  and  $F_z(\omega_i) = [1 + r_p^{13}(\omega_i)] (n^{[1]}/n^{[2]})^2$ , where  $r_{s/p}^{13}$  are the reflectivity coefficient at the  $\{13\}$  interface for  $s$  and  $p$  polarizations, respectively. More detailed expressions may be found in the literature.<sup>4,54,59</sup> For an electromagnetic plane wave, when the electric field is polarized along  $\hat{\mathbf{s}}_i$  (resp. along  $\hat{\mathbf{p}}_i$ ), the magnetic field is polarized along  $-\hat{\mathbf{p}}_i$  (resp. along  $\hat{\mathbf{s}}_i$ ). In other words, the magnetic field is polarized along  $\hat{\mathbf{e}}^{[1],B}(\omega_i) = \hat{\mathbf{k}}_i \times \hat{\mathbf{e}}^{[1]}(\omega_i)$ . We define the

incoming Fresnel factors of the magnetic field  $F^B(\omega_i)$ :

$$B_\alpha(\omega_i) = F_\alpha^B(\omega_i)e_\alpha^{[1],B}(\omega_i)E^0(\omega_i), \quad (\text{C1})$$

with, using Ref. 57 and the formulas of Ref. 4:

$$\begin{aligned} F_x^B(\omega_i) &= \frac{n^{[1]}}{c} [1 - r_s^{13}(\omega_i)], \\ F_y^B(\omega_i) &= \frac{n^{[1]}}{c} [1 + r_p^{13}(\omega_i)], \\ F_z^B(\omega_i) &= \frac{n^{[1]}}{c} [1 + r_s^{13}(\omega_i)]. \end{aligned} \quad (\text{C2})$$

For simplicity, we consider the macroscopic SFG response of layer [2] as described by its surface nonlinear susceptibilities  $\chi^{(2),\text{eee}}$ ,  $\chi^{(2),\text{eem}}$ ,  $\chi^{(2),\text{eme}}$  and  $\chi^{(2),\text{mee}}$ , each being related to one response function  $\beta^{\text{eee}}$ ,  $\beta^{\text{eem}}$ ,  $\beta^{\text{eme}}$  and  $\beta^{\text{mee}}$  through  $\chi^{(2)} = N_s \langle \beta \rangle$ , where  $N_s$  is the surface density of entities and brackets denote appropriate orientation averaging. The nonlinear susceptibilities are the sources of nonlinear polarization  $\mathbf{P}(\omega_3)$  and magnetization  $\mathbf{M}(\omega_3)$  in medium [2]. The Fresnel factors for the reflected SFG beam are defined by:

$$E^0(\omega_3) = \frac{2i\pi\omega_3}{cn_3^{[1]} \cos \theta_3^{[1]}} \sum_\alpha F_\alpha(\omega_3) e_\alpha^{[1]}(\omega_3) P_\alpha^{[2]}(\omega_3), \quad (\text{C3})$$

and:

$$E^0(\omega_3) = \frac{2i\pi\omega_3}{cn_3^{[1]} \cos \theta_3^{[1]}} \sum_\alpha F_\alpha^B(\omega_3) e_\alpha^{[1],B}(\omega_3) M_\alpha^{[2]}(\omega_3), \quad (\text{C4})$$

where it can be checked that the formal expressions for  $F_\alpha(\omega_3)$  and  $F_\alpha^B(\omega_3)$  are identical to their counterparts for  $\omega_1$  and  $\omega_2$  [Eq. (C2)]: the universality of the three Fresnel factors also applies to the magnetic components. Finally, the SFG intensity, as measured by the experimenter, reads:

$$I(\omega_3) = \frac{8\pi^3(\omega_3)^2}{c^3 n_3^{[1]} n_1^{[1]} n_2^{[1]} (\cos \theta_3^{[1]})^2} |\chi_{eff}^{(2)}|^2 I(\omega_1) I(\omega_2), \quad (\text{C5})$$

wherein the quantity  $\chi_{eff}^{(2)}$  including electric and magnetic contributions is defined by:

$$\begin{aligned}
\chi_{eff}^{(2)} &= \sum_{\alpha\beta\gamma} F_\alpha(\omega_3)e_\alpha^{[1]}(\omega_3) F_\beta(\omega_1)e_\beta^{[1]}(\omega_1) F_\gamma(\omega_2)e_\gamma^{[1]}(\omega_2) \chi_{\alpha\beta\gamma}^{(2),eee} \\
&+ F_\alpha(\omega_3)e_\alpha^{[1]}(\omega_3) F_\beta(\omega_1)e_\beta^{[1]}(\omega_1) F_\gamma^B(\omega_2)e_\gamma^{[1],B}(\omega_2) \chi_{\alpha\beta\gamma}^{(2),eem} \\
&+ F_\alpha(\omega_3)e_\alpha^{[1]}(\omega_3) F_\beta^B(\omega_1)e_\beta^{[1],B}(\omega_1) F_\gamma(\omega_2)e_\gamma^{[1]}(\omega_2) \chi_{\alpha\beta\gamma}^{(2),eme} \\
&+ F_\alpha^B(\omega_3)e_\alpha^{[1],B}(\omega_3) F_\beta(\omega_1)e_\beta^{[1]}(\omega_1) F_\gamma(\omega_2)e_\gamma^{[1]}(\omega_2) \chi_{\alpha\beta\gamma}^{(2),mee}. \tag{C6}
\end{aligned}$$

## Appendix D: Equivalence with traceless quadrupole moment

To demonstrate the equivalence between our description of (eQ) couplings based on  $\mathbf{W}^{eQ}$  and that of A. B. Evlyukhin *et al.*<sup>50,60</sup>, we first write  $W_{l\zeta h}^{eQ} = W_{hl\zeta}^{Qe}$  in a compact form:

$$W_{l\zeta h}^{eQ}(\omega, \mathbf{R}) = \hat{R}_h \delta_{l\zeta} X_{16} \left( \frac{\omega |\mathbf{R}|}{c} \right) + \hat{R}_h \hat{R}_l \hat{R}_\zeta X_{17} \left( \frac{\omega |\mathbf{R}|}{c} \right) + (\delta_{h\zeta} \hat{R}_l + \delta_{hl} \hat{R}_\zeta) X_{18} \left( \frac{\omega |\mathbf{R}|}{c} \right), \tag{D1}$$

where  $X_{16}$ ,  $X_{17}$  and  $X_{18}$  are the polynomials in brackets in Eqs. (16), (17) and (18), respectively, weighted by factor  $e^{i\omega |\mathbf{R}|/c}/8\pi\epsilon_0 |\mathbf{R}|^4$ . According to Eqs. (7) and (23) in Refs. 60 and 50, the quadrupolar Green's tensor  $\mathbf{G}^Q$  reads:

$$G_{ij}^Q = \frac{\epsilon_0 c^2}{3\omega^2} \left[ \delta_{ij} (X_{16} + X_{18}) + \hat{R}_i \hat{R}_j X_{17} \right]. \tag{D2}$$

From Eq. (D1), we have:

$$\sum_{h,\zeta} W_{l\zeta h}^{eQ} q_{\zeta h} = \sum_{h,\zeta} \left[ \hat{R}_h \delta_{l\zeta} (X_{16} + X_{18}) + \hat{R}_h \hat{R}_l \hat{R}_\zeta X_{17} \right] q_{\zeta h} + \hat{R}_l (\text{Tr } \mathbf{q}) X_{18}, \tag{D3}$$

where we used the identity  $\sum_{h,\zeta} \delta_{h\zeta} q_{\zeta h} = \text{Tr } \mathbf{q}$ . To relate it to  $\mathbf{G}^Q$  and  $\mathbf{q}' = 3\mathbf{q} - (\text{Tr } \mathbf{q}) \mathbf{1}$ , we compute:

$$\frac{\omega^2}{\epsilon_0 c^2} \sum_{h,\zeta} G_{l\zeta}^Q \hat{R}_h [3q_{\zeta h} - (\text{Tr } \mathbf{q}) \delta_{\zeta h}] = \frac{3\omega^2}{\epsilon_0 c^2} \sum_{h,\zeta} G_{l\zeta}^Q \hat{R}_h q_{\zeta h} - \frac{\omega^2}{\epsilon_0 c^2} (\text{Tr } \mathbf{q}) \sum_h G_{lh}^Q \hat{R}_h. \tag{D4}$$

We can identify the right-hand sides of Eqs. (D3) and (D4). Using Eq. (D2), the first sums over  $h$  and  $\zeta$  are equal in both equations. As for the second sum in Eq. (D4), over  $h$ , we

can check that:

$$\frac{\omega^2}{\varepsilon_0 c^2} (\text{Tr } \mathbf{q}) \sum_h G_{lh}^{\text{Q}} \hat{R}_h = -\hat{R}_l (\text{Tr } \mathbf{q}) X_{18}, \quad (\text{D5})$$

where we used  $\sum_h \hat{R}_h^2 = 1$  and  $X_{16} + X_{17} + X_{18} = -3X_{18}$ . We thus retrieve the second term of Eq. (D3) and demonstrate Eq. (22).

## DATA AVAILABILITY

The data that support the findings of this study are available from the corresponding author upon reasonable request.

## REFERENCES

- <sup>1</sup>J. Hunt, P. Guyot-Sionnest, and Y. Shen, Chem. Phys. Lett. **133**, 189 (1987).
- <sup>2</sup>H. Held, A. I. Lvovsky, X. Wei, and Y. R. Shen, Phys. Rev. B **66**, 205110 (2002).
- <sup>3</sup>M. S. Azam, C. Cai, and D. K. Hore, J. Phys. Chem. C **123**, 23535 (2019).
- <sup>4</sup>B. Busson, J. Chem. Phys. **159**, 034705 (2023).
- <sup>5</sup>A. Lagutchev, S. A. Hambir, and D. D. Dlott, J. Phys. Chem. C **111**, 13645 (2007).
- <sup>6</sup>A. Le Rille and A. Tadjeddine, J. Electroanal. Chem. **467**, 238 (1999).
- <sup>7</sup>G. Gonella, C. Lütgebaucks, A. G. F. de Beer, and S. Roke, J. Phys. Chem. C **120**, 9165 (2016).
- <sup>8</sup>M. Cho, C. Hess, and M. Bonn, Phys. Rev. B **65**, 205423 (2002).
- <sup>9</sup>L. Dalstein, C. Humbert, M. Ben Haddada, S. Boujday, G. Barbillon, and B. Busson, J. Phys. Chem. Lett. **10**, 7706 (2019).
- <sup>10</sup>T. Noblet, L. Dreesen, S. Boujday, C. Méthivier, B. Busson, A. Tadjeddine, and C. Humbert, Commun. Chem. **1**, 76 (2018).
- <sup>11</sup>T. Noblet, B. Busson, and C. Humbert, Phys. Rev. A **104**, 063504 (2021).
- <sup>12</sup>T. Noblet and B. Busson, Phys. Rev. B **105**, 205420 (2022).
- <sup>13</sup>H. DeVoe, J. Chem. Phys. **43**, 3199 (1965).
- <sup>14</sup>B. Busson and L. Dalstein, J. Phys. Chem. C **123**, 26597 (2019).
- <sup>15</sup>R. E. Raab and O. L. de Lange, *Multipole theory in electromagnetism* (Oxford University Press, Oxford, 2005).

- <sup>16</sup>M. Born and E. Wolf, eds., *Principles of Optics*, 7th ed. (Cambridge University Press, 1999).
- <sup>17</sup>J. A. Maytorena, B. S. Mendoza, and W. L. Mochán, *Phys. Rev. B* **57**, 2569 (1998).
- <sup>18</sup>L. Wang, W. Mori, A. Morita, M. Kondoh, M. Okuno, and T.-A. Ishibashi, *J. Phys. Chem. Lett.* **11**, 8527 (2020).
- <sup>19</sup>C. J. Moll, J. Versluis, and H. J. Bakker, *J. Phys. Chem. B* **126**, 270 (2022).
- <sup>20</sup>V. L. Brudny, B. S. Mendoza, and W. Luis Mochán, *Phys. Rev. B* **62**, 11152 (2000).
- <sup>21</sup>E. C. Hao, G. C. Schatz, R. C. Johnson, and J. T. Hupp, *J. Chem. Phys.* **117**, 5963 (2002).
- <sup>22</sup>J. I. Dadap, J. Shan, and T. F. Heinz, *J. Opt. Soc. Am. B* **21**, 1328 (2004).
- <sup>23</sup>J. Nappa, I. Russier-Antoine, E. Benichou, C. Jonin, and P. F. Brevet, *J. Chem. Phys.* **125**, 184712 (2006).
- <sup>24</sup>A. Kundu, S. Tanaka, T. Ishiyama, M. Ahmed, K.-I. Inoue, S. Nihonyanagi, H. Sawai, S. Yamaguchi, A. Morita, and T. Tahara, *J. Phys. Chem. Lett.* **7**, 2597 (2016).
- <sup>25</sup>M. Ahmed, S. Nihonyanagi, A. Kundu, S. Yamaguchi, and T. Tahara, *J. Phys. Chem. Lett.* **11**, 9123 (2020).
- <sup>26</sup>C. J. Moll, J. Versluis, and H. J. Bakker, *Phys. Rev. Lett.* **127**, 116001 (2021).
- <sup>27</sup>T. Seki, C.-C. Yu, K.-Y. Chiang, J. Tan, S. Sun, S. Ye, M. Bonn, and Y. Nagata, *J. Phys. Chem. B* **125**, 7060 (2021).
- <sup>28</sup>Y. R. Shen, *J. Phys. Chem. C* **116**, 15505 (2012).
- <sup>29</sup>W.-C. Yang, B. Busson, and D. K. Hore, *J. Chem. Phys.* **152**, 084708 (2020).
- <sup>30</sup>X. Wei, S.-C. Hong, A. I. Lvovsky, H. Held, and Y. R. Shen, *J. Phys. Chem. B* **104**, 3349 (2000).
- <sup>31</sup>B. Busson, *J. Chem. Phys.* **159**, 034707 (2023).
- <sup>32</sup>S. Yamaguchi, K. Shiratori, A. Morita, and T. Tahara, *J. Chem. Phys.* **134**, 184705 (2011).
- <sup>33</sup>K. Matsuzaki, S. Nihonyanagi, S. Yamaguchi, T. Nagata, and T. Tahara, *J. Phys. Chem. Lett.* **4**, 1654 (2013).
- <sup>34</sup>B. S. Mendoza, W. L. Mochán, and J. A. Maytorena, *Phys. Rev. B* **60**, 14334 (1999).
- <sup>35</sup>E. U. Condon, *Rev. Mod. Phys.* **9**, 432 (1937).
- <sup>36</sup>G. Snatzke, in *Circular Dichroism: Principles and Applications*, edited by N. Berova, K. Nakanishi, and R. W. Woody (Wiley, New York, 2000) Chap. 1, pp. 1–35.

- <sup>37</sup>F. Hache, H. Mesnil, and M. C. Schanne-Klein, *J. Chem. Phys.* **115**, 6707 (2001).
- <sup>38</sup>J. A. Schellman, *Acc. Chem. Res.* **1**, 144 (1968).
- <sup>39</sup>D. P. Craig and T. Thirunamachandran, *Molecular quantum electrodynamics: an introduction to radiation-molecule interaction* (Academic Press, 1984).
- <sup>40</sup>I. Tinoco Jr., “Theoretical aspects of optical activity part two: Polymers,” in *Adv. Chem. Phys.* (John Wiley and Sons, Ltd, 1962) pp. 113–160.
- <sup>41</sup>L. D. Landau and E. M. Lifshitz, *Quantum Mechanics* (Pergamon, 1977).
- <sup>42</sup>M. Combescot, S.-Y. Shiao, and V. Voliotis, *Phys. Rev. B* **99**, 245202 (2019).
- <sup>43</sup>G. D. Scholes, A. H. A. Clayton, and K. P. Ghiggino, *J. Chem. Phys.* **97**, 7405 (1992).
- <sup>44</sup>D. P. Craig and T. Thirunamachandran, *Theor. Chem. Acc.* **102**, 112 (1999).
- <sup>45</sup>S. Sioncke, T. Verbiest, and A. Persoons, *Mat. Sci. Engin. Rep.* **42**, 115 (2003).
- <sup>46</sup>Y. Tang and A. E. Cohen, *Phys. Rev. Lett.* **104**, 163901 (2010).
- <sup>47</sup>M. Nieto-Vesperinas, *Phys. Rev. A* **100**, 023812 (2019).
- <sup>48</sup>A. Patoux, C. Majorel, P. R. Wiecha, A. Cuche, O. L. Muskens, C. Girard, and A. Arbouet, *Phys. Rev. B* **101**, 235418 (2020).
- <sup>49</sup>A. Alù and N. Engheta, *Phys. Rev. B* **79**, 235412 (2009).
- <sup>50</sup>A. B. Evlyukhin, C. Reinhardt, U. Zywiets, and B. N. Chichkov, *Phys. Rev. B* **85**, 245411 (2012).
- <sup>51</sup>M. Kauranen, T. Verbiest, J. J. Maki, and A. Persoons, *J. Chem. Phys.* **101**, 8193 (1994).
- <sup>52</sup>M. Kauranen, T. Verbiest, and A. Persoons, *J. Modern Opt.* **45**, 403 (1998).
- <sup>53</sup>L. Dalstein, A. Revel, C. Humbert, and B. Busson, *J. Chem. Phys.* **148**, 134701 (2018).
- <sup>54</sup>X. Zhuang, P. B. Miranda, D. Kim, and Y. R. Shen, *Phys. Rev. B* **59**, 12632 (1999).
- <sup>55</sup>B. Busson, *J. Chem. Phys.* **159**, 034706 (2023).
- <sup>56</sup>D. B. O’Brien and A. M. Massari, *J. Chem. Phys.* **142**, 024704 (2015).
- <sup>57</sup>J. J. Maki, M. Kauranen, and A. Persoons, *Phys. Rev. B* **51**, 1425 (1995).
- <sup>58</sup>J. D. Jackson, ed., *Classical Electrodynamics*, 3rd ed. (Wiley, 1999).
- <sup>59</sup>T. F. Heinz, in *Nonlinear Surf. Electromagn. Phenom.*, edited by H. E. Ponath and G. I. Stegeman (Elsevier, Amsterdam, 1991) Chap. 5, pp. 353–416.
- <sup>60</sup>A. B. Evlyukhin, C. Reinhardt, and B. N. Chichkov, *Phys. Rev. B* **84**, 235429 (2011).
- <sup>61</sup>K. Matsumori, R. Fujimura, and M. Retsch, *J. Phys. Chem. C* **127**, 19127 (2023).
- <sup>62</sup>A. G. F. de Beer and S. Roke, *J. Chem. Phys.* **132**, 234702 (2010).

- <sup>63</sup>H. B. de Aguiar, R. Scheu, K. C. Jena, A. G. F. de Beer, and S. Roke, *Phys. Chem. Chem. Phys.* **14**, 6826 (2012).
- <sup>64</sup>P. Fischer, A. D. Buckingham, and A. C. Albrecht, *Phys. Rev. A* **64**, 053816 (2001).
- <sup>65</sup>P. Fischer, F. W. Wise, and A. C. Albrecht, *J. Phys. Chem. A* **107**, 8232 (2003).
- <sup>66</sup>M. Okuno and T.-A. Ishibashi, *J. Chem. Phys.* **149**, 244703 (2018).
- <sup>67</sup>M. A. Belkin, T. A. Kulakov, K. H. Ernst, L. Yan, and Y. R. Shen, *Phys. Rev. Lett.* **85**, 4474 (2000).
- <sup>68</sup>J. A. Giordmaine, *Phys. Rev.* **138**, A1599 (1965).
- <sup>69</sup>F. G. Fumi, *Acta Cryst.* **5**, 44 (1952).
- <sup>70</sup>N. G. Bastús, J. Piella, and V. Puntès, *Langmuir* **32**, 290 (2016).
- <sup>71</sup>G. Mie, *Annalen der Physik* **330**, 377 (1908).
- <sup>72</sup>C. P. Burrows and W. L. Barnes, *Opt. Express* **18**, 3187 (2010).
- <sup>73</sup>F. Hao, E. M. Larsson, T. A. Ali, D. S. Sutherland, and P. Nordlander, *Chem. Phys. Lett.* **458**, 262 (2008).
- <sup>74</sup>Q. Sun, H. Yu, K. Ueno, A. Kubo, Y. Matsuo, and H. Misawa, *ACS Nano* **10**, 3835 (2016).
- <sup>75</sup>R. Esteban, R. Vogelgesang, J. Dorfmueller, A. Dmitriev, C. Rockstuhl, C. Etrich, and K. Kern, *Nano Letters* **8**, 3155 (2008).
- <sup>76</sup>M. J. Stephen, *Math. Proc. Cambridge Phil. Soc.* **54**, 81 (1958).
- <sup>77</sup>C. F. Bohren and D. R. Huffman, *Absorption and scattering of light by small particles* (Wiley, 1983).
- <sup>78</sup>M. Kauranen, J. J. Maki, T. Verbiest, S. Van Elshocht, and A. Persoons, *Phys. Rev. B* **55**, R1985 (1997).
- <sup>79</sup>F. Matsumura, C.-C. Yu, X. Yu, K.-Y. Chiang, T. Seki, M. Bonn, and Y. Nagata, *J. Phys. Chem. B* **127**, 5288 (2023).
- <sup>80</sup>Y. R. Shen, *The Principles of Nonlinear Optics* (Wiley, New York, USA, 1984).
- <sup>81</sup>R. W. Boyd, *Nonlinear optics* (Academic Press, San Diego, CA, USA, 2003).
- <sup>82</sup>S. S. Andrews, *J. Chem. Educ.* **81**, 877 (2004).
- <sup>83</sup>S. Roy, K.-K. Hung, U. Stege, and D. K. Hore, *Appl. Spectrosc. Rev.* **49**, 233 (2014).
- <sup>84</sup>Y. He, H. Ren, E.-M. You, P. M. Radjenovic, S.-G. Sun, Z.-Q. Tian, J.-F. Li, and Z. Wang, *Phys. Rev. Lett.* **125**, 047401 (2020).

- <sup>85</sup>P. D. Terekhov, K. V. Baryshnikova, Y. A. Artemyev, A. Karabchevsky, S. A. S., and A. B. Evlyukhin, *Phys. Rev. B* **96**, 035443 (2017).
- <sup>86</sup>A. Alabastri, X. Yang, A. Manjavacas, H. O. Everitt, and P. Nordlander, *ACS Nano* **10**, 4835 (2016).
- <sup>87</sup>R. Baer and E. Rabani, *J. Chem. Phys.* **128**, 184710 (2008).
- <sup>88</sup>E. Hao and G. C. Schatz, *J. Chem. Phys.* **120**, 357 (2004).
- <sup>89</sup>X. Zhang, X. Leng, H. Yin, and Y. Ma, *J. Phys. Chem. C* **125**, 17861 (2021).
- <sup>90</sup>G. D. Scholes, X. J. Jordanides, and G. R. Fleming, *J. Phys. Chem. B* **105**, 1640 (2001).
- <sup>91</sup>S. P. Hastings, P. Swanglap, Z. Qian, Y. Fang, S.-J. Park, S. Link, N. Engheta, and Z. Fakhraai, *ACS Nano* **8**, 9025 (2014).
- <sup>92</sup>T. Kawaguchi, K. Shiratori, Y. Henmi, T. Ishiyama, , and A. Morita, *J. Phys. Chem. C* **116**, 13169 (2012).
- <sup>93</sup>C. Katan, S. Tretiak, M. H. V. Werts, A. J. Bain, R. J. Marsh, N. Leonczek, N. Nicolaou, E. Badaeva, O. Mongin, and M. Blanchard-Desce, *J. Phys. Chem. B* **111**, 9468 (2007).
- <sup>94</sup>K. Susumu, J. A. N. Fisher, J. Zheng, D. N. Beratan, and M. J. Yodh, A. G. and Therien, *J. Phys. Chem. A* **115**, 5525 (2011).
- <sup>95</sup>S. Hahn, , D. Kim, and M. Cho, *J. Phys. Chem. B* **103**, 8221 (1999).
- <sup>96</sup>M. Barzoukas and M. Blanchard-Desce, *J. Chem. Phys.* **113**, 3951 (2000).
- <sup>97</sup>M. Yang, S. Li, J. Ma, and Y. Jiang, *Chemical Physics Letters* **354**, 316 (2002).
- <sup>98</sup>P. K. Das, *J. Phys. Chem. B* **110**, 7621 (2006).
- <sup>99</sup>G. Revillod, J. Duboisset, I. Russier-Antoine, E. Benichou, G. Bachelier, C. Jonin, and P.-F. Brevet, *J. Phys. Chem. C* **112**, 2716 (2008).
- <sup>100</sup>R.-P. Pan, H. D. Wei, and Y. R. Shen, *Phys. Rev. B* **39**, 1229 (1989).
- <sup>101</sup>J. S. Garitaonandia, M. Insausti, E. Goikolea, M. Suzuki, J. D. Cashion, N. Kawamura, H. Ohsawa, I. Gil de Muro, K. Suzuki, F. Plazaola, and T. Rojo, *Nano Letters* **8**, 661 (2008).
- <sup>102</sup>J. Foxley and K. L. Knappenberger, *Ann. Rev. Phys. Chem.* **74**, 53 (2023).
- <sup>103</sup>V. Rodriguez, *J. Chem. Phys.* **128**, 064707 (2008).
- <sup>104</sup>A. Moscovitz, "Theoretical aspects of optical activity part one: Small molecules," in *Advances in Chemical Physics* (John Wiley, 1962) pp. 67–112.
- <sup>105</sup>J. Applequist, *J. Chem. Phys.* **58**, 4251 (1973).

- <sup>106</sup>D. S. Kliger, J. W. Lewis, and C. E. Randall, *Polarized Light in Optics and Spectroscopy* (Academic Press, 1990) p. 804.
- <sup>107</sup>J. A. Schellman, *Chem. Rev.* **75**, 323 (1975).
- <sup>108</sup>A. Kosłowski, N. Sreerama, and R. W. Woody, in *Circular Dichroism: Principles and Applications*, edited by N. Berova, K. Nakanishi, and R. W. Woody (Wiley, New York, 2000) Chap. 3, pp. 55–96.
- <sup>109</sup>T. Verbiest, M. Kauranen, Y. Van Rompaey, and A. Persoons, *Phys. Rev. Lett.* **77**, 1456 (1996).
- <sup>110</sup>B. J. Burke, A. J. Moad, M. A. Polizzi, and G. J. Simpson, *J. Am. Chem. Soc.* **125**, 9111 (2003).
- <sup>111</sup>M. Hayashi, S. H. Lin, and Y. R. Shen, *J. Phys. Chem. A* **108**, 8058 (2004).
- <sup>112</sup>G. J. Simpson, *ChemPhysChem* **5**, 1301 (2004).
- <sup>113</sup>H. Hoshi, T. Yamada, K. Ishikawa, H. Takezoe, and A. Fukuda, *Phys. Rev. B* **52**, 12355 (1995).
- <sup>114</sup>S. Van Elshocht, T. Verbiest, M. Kauranen, A. Persoons, B. M. W. Langeveld-Voss, and E. W. Meijer, *J. Chem. Phys.* **107**, 8201 (1997).
- <sup>115</sup>M. C. Schanne-Klein, F. Hache, A. Roy, C. Flytzanis, and C. Payrastré, *J. Chem. Phys.* **108**, 9436 (1998).
- <sup>116</sup>J. J. Maki, M. Kauranen, T. Verbiest, and A. Persoons, *Phys. Rev. B* **55**, 5021 (1997).
- <sup>117</sup>J. J. Maki and A. Persoons, *J. Chem. Phys.* **104**, 9340 (1996).
- <sup>118</sup>M. Belkin, Y. Shen, and C. Flytzanis, *Chem. Phys. Lett.* **363**, 479 (2002).
- <sup>119</sup>P. Fischer and F. Hache, *Chirality* **17**, 421 (2005).
- <sup>120</sup>M. L. McDermott and P. B. Petersen, *J. Phys. Chem. B* **119**, 12417 (2015).
- <sup>121</sup>E. A. Perets, P. E. Videla, E. C. Y. Yan, and V. S. Batista, *J. Phys. Chem. B* **123**, 5769 (2019).
- <sup>122</sup>S. Strazdaite, S. J. Roeters, A. Sakalauskas, T. Sneideris, J. Kirschner, K. B. Pedersen, B. Schiøtt, F. Jensen, T. Weidner, V. Smirnovas, and G. Niaura, *J. Phys. Chem. B* **125**, 11208 (2021).
- <sup>123</sup>G. Y. Stokes, J. M. Gibbs-Davis, F. C. Boman, B. R. Stepp, A. G. Condie, S. T. Nguyen, and F. M. Geiger, *J. Am. Chem. Soc.* **129**, 7492 (2007).
- <sup>124</sup>Y. Zhang, X. Qin, X. Zhu, M. Liu, Y. Guo, and Z. Zhang, *Nature Comm.* **13**, 7737 (2022).

- <sup>125</sup>J. D. Byers, H. I. Yee, and J. M. Hicks, *J. Chem. Phys.* **101**, 6233 (1994).
- <sup>126</sup>T. Petralli-Mallow, T. M. Wong, J. D. Byers, H. I. Yee, and J. M. Hicks, *J. Phys. Chem.* **97**, 1383 (1993).
- <sup>127</sup>J. J. Maki, T. Verbiest, M. Kauranen, S. V. Elshocht, and A. Persoons, *J. Chem. Phys.* **105**, 767 (1996).
- <sup>128</sup>J.-H. Choi, S. Cheon, and M. Cho, *J. Chem. Phys.* **132**, 074506 (2010).
- <sup>129</sup>M. A. Belkin and Y. R. Shen, *Phys. Rev. Lett.* **91**, 213907 (2003).
- <sup>130</sup>L. Rosenfeld, *Z. Physik* **52**, 161 (1929).
- <sup>131</sup>E. A. Power and R. Shail, *Math. Proc. Cambridge Phil. Soc.* **55**, 87– (1959).
- <sup>132</sup>W. Kuhn, *Z. Phys. Chem.* **4B**, 14 (1929).
- <sup>133</sup>P. M. Bayley, E. B. Nielsen, and J. A. Schellman, *J. Phys. Chem.* **73**, 228 (1969).
- <sup>134</sup>J. G. Kirkwood, *J. Chem. Phys.* **5**, 479 (1937).
- <sup>135</sup>W. Moffitt, *J. Chem. Phys.* **25**, 467 (1956).
- <sup>136</sup>S. Davydov, *Theory of Molecular Excitons* (Plenum Press, New York, NY, USA, 1971).
- <sup>137</sup>D. Haase, *Theoret. Chim. Acta* **64**, 421 (1984).
- <sup>138</sup>S. Superchi, E. Giorgio, and C. Rosini, *Chirality* **16**, 422 (2004).
- <sup>139</sup>X. Yin, M. Schäferling, B. Metzger, and H. Giessen, *Nano Letters* **13**, 6238 (2013).
- <sup>140</sup>M. A. Belkin, S. H. Han, X. Wei, and Y. R. Shen, *Phys. Rev. Lett.* **87**, 113001 (2001).
- <sup>141</sup>M. A. Belkin, Y. R. Shen, and R. A. Harris, *J. Chem. Phys.* **120**, 10118 (2004).
- <sup>142</sup>R.-H. Zheng, D.-M. Chen, W.-M. Wei, T.-J. He, and F.-C. Liu, *J. Phys. Chem. B* **110**, 4480 (2006).
- <sup>143</sup>A. Morita, *Chem. Phys. Lett.* **398**, 361 (2004).
- <sup>144</sup>C. Neipert, B. Space, and A. B. Roney, *J. Phys. Chem. C* **111**, 8749 (2007).
- <sup>145</sup>Y. T. Lam and T. Thirunamachandran, *J. Chem. Phys.* **77**, 3810 (1982).
- <sup>146</sup>G. Wagnière, *J. Chem. Phys.* **77**, 2786 (1982).
- <sup>147</sup>N. Bloembergen, R. K. Chang, S. S. Jha, and C. H. Lee, *Phys. Rev.* **174**, 813 (1968).
- <sup>148</sup>A. Perry, C. Neipert, and B. Space, *Chem. Rev.* **106**, 1234 (2006).